Magnetic Resonance Imaging, Vol. 9, pp. 1-37, 1991
Printed in the USA.

0730-725X/91 $3.00 + .00

ULTRA-FAST IMAGING

MARK S. COHEN, PH.D. AND ROBERT M. WEISSKOFF, PH.D.

Advanced NMR Systems, Inc., 30 Sonar Drive, Woburn, Massachusetts 02129, USA

The relatively long scan times with currently available technology restrict the range of MRI applications, increase the cost of scanning by limiting throughput, and lead to image artifacts from patient motion during scans. Ultra-fast imaging, in several guises, is now poised for introduction into clinical practice. With the Instascan method, a descendant of the echo planar technique, complete MR images may be obtained hundreds to thousands of times faster than in conventional approaches and now yield spatial resolution and contrast directly comparable to standard MRI. "Single-shot" imaging methods, such as Instascan, are utilized in the study of dynamic processes, in the direct evaluation of motion (as in diffusion sensitive imaging), and in dramatic new applications including the interactive control of intraparenchymal laser surgery. Improvements to the small flip angle method, FLASH, have also pushed scan times into the sub-second domain; this method may be implemented on presently available imaging equipment but yields contrast behavior different from the traditional spin echo techniques and displays signal-to-noise ratios significantly lower than single-shot imaging. Ultimately, incorporating ultra-fast MR imaging techniques into the armamentarium of the radiologist will likely require changes to many aspects of the MRI practice, from expanded involvement with the scan process to management of the increased data load, and may lead to dramatic changes in the scope of the MRI practice.

Keywords: **NMR; Magnetic resonance imaging (MRI); Echo planar imaging; Instascan; Fast imaging.**

INTRODUCTION

Magnetic resonance imaging (MRI) has proven to be an extremely sensitive and increasingly specific modality for *in vivo* diagnostic scanning. Yet, for all its efficacy, MRI remains costly (1) and cumbersome and MRI scan times, that are long compared to physiological motion and patient tolerance, have ultimately limited its use and acceptance. In this paper we discuss emerging technologies in magnetic resonance imaging that drastically reduce scan times. Conventional MR methods build images from repeated excitations and sampling of the MR data. While considerable progress has been made over the past few years on gradient echo methods that speed this process, particular attention will be paid here to so-called single-shot imaging methods with which complete images are formed following a single excitation. In the present review, *ultra*-fast imaging refers to scan times short compared to physiological motion, typically less than a hundred milliseconds or so. The bulk of this paper, therefore, addresses the "instant" methods, particularly Instascan, with which complete MR images are acquired in as little as 1/30th of a second. Our discussion of instant imaging will address both implementation principles and applications of this novel method.

In section 1, to motivate the discussion for ultra-fast imaging, we will discuss some of the limitations of contemporary scanning technology, particularly those related to scanning times *per se*. Section 2 reviews the history and technological basis of the single-shot imaging method known as Instascan. To clarify the ensuing discussion of the method, we review the *k*-space formalism for describing the MR raw data and we will

RECEIVED 8/1/90; ACCEPTED 9/17/90.

Acknowledgements – The development of the Instascan system and its many new applications is the result of the collective effort of a large number of people. The authors wish to acknowledge the extensive contributions made by the staff at Advanced NMR Systems, Inc., especially by Richard Rzedzian and Ian Pykett and by our many collaborators at the Harvard Medical School, particularly Bruce Rosen, Jack Belliveau, Robert McKinstry, Tom Brady, Howard Kantor, and J. Michael Vevea at the Massachusetts General Hospital and, at the Brigham and Women's Hospital, Ferenc Jolesz and Alan Bleier. For allowing us to present the results of their own work we thank Jens Frahm and Craig Meyer, and for her many helpful comments on the manuscript our sincere thanks to Joyce Roop.

Address all correspondence to Mark S. Cohen, Ph.D., Technical Director of Clinical NMR, MGH Imaging Center, Building 149, 13th Street, Charlestown, MA 02129, USA.

rely heavily (though informally) on that concept to present recent advances in spatial resolution and control of imaging parameters. Physical, technical and safety limitations of single-shot imaging are also discussed in this section. Both tested and emerging clinical applications of Instascan are discussed in section 3, indicating some of the potential of ultra-fast imaging. As single-shot imaging has developed greatly in recent years, so too have other speed enhancement methods. Some, particularly FLASH imaging, have progressed to the point that they also have become ultra-fast technologies. The basic principles underlying these low flip angle methods are reviewed in section 4, and a variety of high speed techniques are compared and contrasted in this section. Finally, section 5 explores the future of ultra-fast MRI.

1. MOTIVATIONS FOR HIGH SPEED IMAGING

Of the commonly available diagnostic imaging examinations (e.g. ultra-sound, fluoroscopy, computed tomography, nuclear medicine etc…) magnetic resonance ranks among the slowest. The long scan times of MRI are justified only by the high quality and diagnostic efficacy of the images. We identify three main deleterious consequences of these long scan times: imaging artifacts, limitations on the range of applications, and increased cost. Each provides impetus for the development of high-speed scanning alternatives.

1.1 Artifacts

1.1.1 *Physiological Motion.* Many normal physiological processes take place rapidly compared to the several minutes needed to produce a conventional MR image. Respiration, pulsation, peristalsis and other movements that occur during the exam can result in substantial distortion of the MR image. Because of the Fourier encoding process used in MR imaging, motion produces gross artifacts (Figure 1) that can obscure the whole image and corrupt its contrast (2, 3). While some of the more pronounced effects of simple motions, such as blood flow, can be attenuated by various motion compensation schemes (4) even the best schemes cannot prevent blurring.

For certain cyclical motions (e.g. respiration and pulsation) it is possible to synchronize the MR data acquisition with the source of the motion itself, by such means as ECG triggering or respiratory gating. Though these methods can be remarkably effective, they can make scan setup more complex. In addition, they result in contrast distortion; in cardiac triggered scans TR, for example, is determined by the patient's heart rate, which may itself be irregular (5).

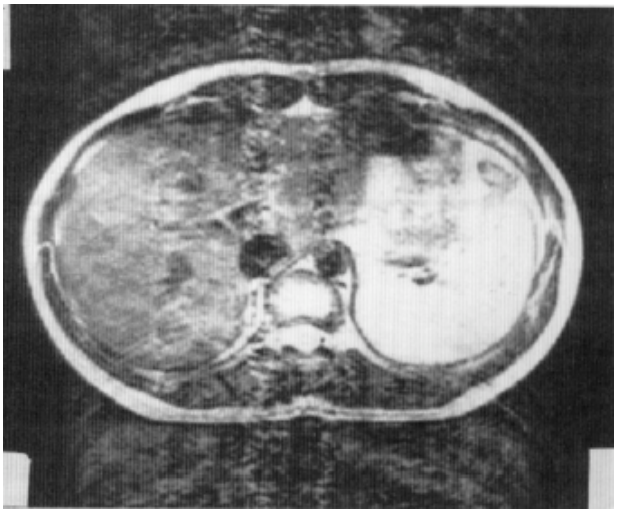

Fig. 1. Conventionally acquired MRI scan of the abdomen. Because scan times are relatively long compared to normal physiological motion such as breathing, image artifacts tend to accumulate during the scan. Due to the Fourier-encoding process used in the collection of conventional MR data, however, the resulting artifacts are not simply a blurring of the image. Instead, as shown here, even simple motion of the chest wall results in gross contamination of the image, with artifacts extending well away from the moving tissue. Note also that the image contrast may be obscured (as in the anterior portion of the liver) because of the signal displacement. TR: 2000 msec, TE: 20 msec, slice thickness: 10 mm

1.1.2 *Patient Motion.* Due to the motion sensitivity of conventional MRI, to obtain high quality images the patient must remain perfectly still for the entire acquisition of a single image. Artifacts from patient motion reduce the diagnostic yield of MR scans substantially, particularly for those exams, such as cervical and lumbar spine, where pain is the primary symptom and the patient may experience difficulty remaining still. This problem is exacerbated in hospital-based centers that often serve a high proportion of non-ambulatory patients. Due to claustrophobia, as many as 15% of patients refuse MR scans, or are not sufficiently cooperative to produce diagnostic images. It is likely that the claustrophobia is aggravated by long exam times.

1.2 Applications Range

Despite its high intrinsic tissue contrast and proven sensitivity to a wide variety of pathological conditions, the majority of clinical MRI is still limited to the central nervous system. Of the many factors that account for this, the limitations of MRI in the presence of motion weigh heavily, yet the medical indications for sensitive diagnostic procedures in the abdomen and tho-

rax offer potential areas of growth for MRI. With present technology it is difficult to obtain MR images of the liver, for example, that are reasonably free of artifact. While synchronization to physiological processes, such as cardiac pulsation, may sometimes be used, such techniques are generally impossible in the presence of non-periodic motion, for example peristalsis, or in the imaging of transient events, such as the passage of contrast agents.

Certain emerging technologies, such as single-shot diffusion-sensitive imaging techniques (6, 7) are effectively precluded in combination with conventional acquisitions, due to the extreme motion sensitivity of the techniques (see section 3.4, *"diffusion imaging"*). Many of the more exciting application of single-shot imaging, such as interactive guidance of surgical procedures (see section 3.7), are possible only in combination with extremely rapid imaging. In the future there will be many applications (for example whole body screening) whose medical potential is almost unexplored.

1.3 Cost

The average per-patient charge for a body MRI exam in the U.S. was estimated, in 1985, at $700 (1) including a $516 technical fee and a $184 professional charge, making MR one of the more expensive diagnostic imaging modalities. A major portion of that billed fee is related to the fixed cost of the equipment (which must be amortized across the total number of patients scanned) and to the hourly cost of staffing the instruments. True variable costs (film and other overhead) represent only a fraction of the total costs. A substantial impact of the long MR scan time may therefore be reflected in the cost per scan, since the equipment cost must be recovered by patient billing. It is difficult to estimate the effect that scan time reduction might have on the cost of the examination but it is reasonable to assume that improvements in instrument throughput are likely to result in lowered MR imaging costs per patient.

2. INSTASCAN

2.1 Tissue relaxation times

A key feature of the magnetic resonance (MR) phenomenon is the refractory nature of the MR signal. Samples, biological or otherwise, have unique rate constants (8) that characterized the extent to which the MR signal is reduced by rapid repeated excitations in pulsed experiments (9). This rate constant has subsequently come to be known as T_1 (or the longitudinal relaxation rate). Because T_1 is a tissue-specific property, it is an important determinant of the contrast seen on MR images. The MR phenomenon depends upon quantum properties at the nuclear level, yet the T_1 rate constants are surprisingly long; *in vivo* T_1's range from tens of milliseconds to several seconds (10, 11).

The MR signal is not only diminished by repeated excitations, but decays relatively rapidly at a second tissue-specific rate, known as T_2 (the transverse relaxation rate). Typical *in vivo* T_2's range from a few milliseconds (msec) to a second or so (10, 11). It is this combination of the relatively long T_1 and the short T_2 of biological materials that is responsible for the prolonged imaging times in conventional MRI, that needs multiple excitations to produce single images. For example, these methods require 256 excitations for a 256 × 256 final image. The TR (that is, the repetition time between successive excitations) is typically from 500 msec to 3 seconds; shorter TR's will lead to unacceptable losses in the strength of the MR signal. Imaging times therefore typically range from 2 to 15 minutes.

2.2 Alternative Spatial Encoding Methods

As will be discussed below (cf. section 4.1.1 *"FLASH and Other Small Flip Angle Techniques"*) the small flip angle methods address the issue of scanning speed by reducing the TR while using otherwise conventional data acquisition technology. Several other approaches to spatial encoding have also attained varying degrees of acceptance. To explain these methods, and to aid in discussion of Instascan, we will informally introduce *k*-space, an heuristic used to describe MR raw data as it appears in virtually all contemporary MR instruments.

2.2.1. *K-space Traversals.* The *k*-space method is a useful formalism proposed by Brown *et al.* (12) and developed by Twig (13, 14) and Ljunggren (15), for describing and manipulating the MR raw data collected in the Fourier-encoded scanning methods commonly used in MR imaging. In this formalism the data acquisition and reconstruction are analyzed from the perspective of acquiring spatial frequency data. These data are converted to an image by the Fourier transform. The distance from the origin of *k*-space, and thus the spatial frequency information acquired at any given time, depends solely upon the history of the applied horizontal and vertical gradients, as described in the equation:

$$\boldsymbol{k}_n(t) = \gamma \int_0^t \boldsymbol{G}_n(s)\mathrm{d}s \qquad (1)$$

where $\mathbf{k}_n$ is the *k*-space displacement along the G_n axis, **s** is the spatial frequency and g is the

gyromagnetic ratio. Usually, one axis of *k*-space describes the phase and the other the frequency of the MR signal. Signals corresponding to low spatial frequencies (i.e., large objects) are concentrated near the origin of *k*-space. Information about higher spatial frequencies (e.g. edges and smaller objects) is spread further from the origin: leaving the gradients on for a longer time, or increasing their amplitude, results in better encoding of information from smaller features of the sample. Where the integral of the applied gradients is zero (i.e. where the signal is undisturbed by the gradients) the MR signal is usually at its greatest, for this reason, each time the MR signal crosses either axis in *k*-space it is said to form a "gradient echo".

Every location in *k*-space corresponds to a combination of the integrals of the applied gradients. Since these integrals evolve over time, the position of the MR signal on the *k*-space plane describes a trajectory. If the time spent in spatial encoding is short compared to other temporal factors (such as T_2-related signal decay or patient motion) then the appearance of the final image is independent of the specific *k*-space trajectory. On the other hand, if *k*-space is not completely and/or evenly sampled, various artifacts may appear in the final image (13).

We now present the familiar 2D acquisition method in detail, and show how the process is described in *k*-space (see Figure 2). This description will be particularly important by contrast to the instant strategies discussed below. Following each signal-producing RF pulse, a magnetic field gradient is applied along one axis of the magnet (conventionally called the frequency-encoding, or "readout", direction) that causes the frequency of the MR signal to vary along that axis. While the gradient is applied, a single line of data may then be collected. This line contains spatial information about the sample along only this axis. Because the gradients tend to dephase, and therefore reduce, the MR signal, a "pre-encoding" gradient pulse of opposite polarity is generally applied prior to sampling. The gradient echo thus formed as the trajectory crosses the *k*-frequency axis is generally timed to correspond with the Hahn spin echo. To spatially encode along the orthogonal axis the strategy is slightly modified: a second, independent, gradient (the *phase-encoding* gradient) is pulsed briefly *prior* to data collection (this gradient causes a *phase* distribution of the signal along that direction). That is, each line contains all of the spatial frequency information about one axis for a given spatial frequency along the other. To complete the im-

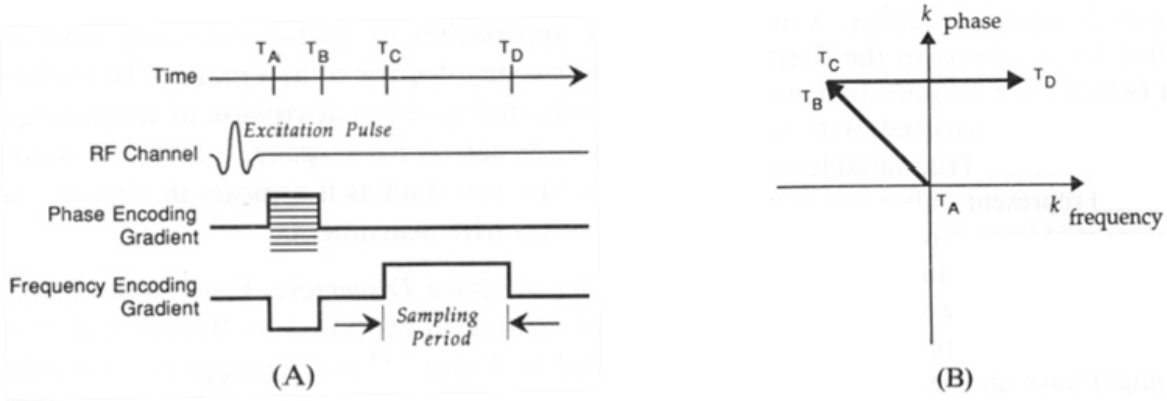

Fig. 2. Spatial encoding scheme used in conventional MRI and its *k*-space representation. (A) Magnetic field gradients are used to add spatial information to the MR signal. Separate gradient systems are used along the two orthogonal axes, conventionally called, "phase encoding" and "frequency encoding." These gradients have the effect of frequency-dispersing the MR signal along their respective axes. Fourier transformation is then used to recover the spatial information. The "pulse sequence" shown is for a FLASH technique, though the gradient scheme and *k*-space trajectory used in spin-echo imaging are similar. (B) *K*-space representation of the pulse sequence shown in (A). The *k*-trajectory is a useful formalism for analyzing the spatial-encoding process. The MR Signal, after gradient encoding, can be seen as a map of spatial frequencies along the gradient axes. To form a complete image it is necessary to collect data from a two-dimensional space (*k-space*) of spatial frequencies along the two orthogonal axes. One way to view this process in MR is to consider the signal to have a position in the complex *k-space* plane given by the integral of the applied gradient along each of the respective gradient axes. The gradient pulses applied between time points T_A and T_B in (A) impart a phase shift of the signal in the complex plane from the origin to the point marked T_B. Between times T_C and T_D a trajectory is made across the plane as shown above and the data for a single line of *k-space* are collected. The next line of data is collected by repeating the entire experiment, but with a pulse of the phase encoding gradient having a different magnitude so that the data have a different displacement along the *k*-phase axis. The experiment is repeated until the plane is symmetrically filled with data points; the two dimensional Fourier transform of this raw data space yields the MR image.

age, the process must be repeated to collect all of the spatial frequencies along the phase axis. In the k-space formalism, a pulse of the phase-encoding gradient gives the data a displacement along the k-phase axis. The frequency-encoding gradient then creates a trajectory along the k-frequency axis. In conventional imagers, it is not generally practical to take more than one line of data following each excitation, because the time to acquire and encode a line of data is typically on the order of ten milliseconds. Taking more than one line per excitation would result in a total signal collection time that is long compared to T_2* – the rate of spontaneous signal decay. The 2D Fourier transform of the collected time data forms the final image.

2.2.2. *Conjugate Synthesis.* The final image from a "real" sample should, theoretically, contain no imaginary component and the signals at +**k** and -**k** should be complex conjugates of one another (16). If the image data truly contained no imaginary component, it would be trivial to calculate the conjugate and therefore it would be necessary to collect the data over only one-half of *k*-space (either +**k** or -**k**) to form a complete image of the real object. Real world effects – imperfect timing, magnetic field inhomogeneity, non-uniform RF penetration, patient motion etc… – always introduce some phase distortion into the image. Generally, therefore, a magnitude image is calculated from the real and imaginary part of the Fourier-transformed *k*-space data. A phase error, not visible in the magnitude images, will still exist due to the non-idealities described above. Generally, most such effects cause a low spatial frequency error. A variety of techniques exist to correct for this, usually involving the sampling of slightly more than half of *k*-space. These extra data are used to measure the phase error, which is then applied as a correction to the image. Such techniques, known as conjugate synthesis (17), have been used to obtain an approximately two-fold reduction in scan time for almost any pulse sequence and are now part of the armamentarium of most commercial scanners.

An important advantage of the conjugate synthesis technique is its ability to cut scan time without compromising image contrast. Collecting just over half number of lines, however, results in an SNR loss of about 30%. The partial sampling of k-space can result also in some additional loss of signal from flowing spins, and in small regions that include substantial susceptibility gradients.

2.3 History

2.3.1. *Echo Planar Imaging.* In 1977, Peter Mansfield (18, 19) proposed the technique known echo-planar imaging or EPI. With this method, the complete 2D encoding process is completed during the free induction decay following a single excitation pulse. In the original implementation, a small gradient was applied along the phase-encoding axis while rapidly alternating pulses were applied with the frequency-encoding gradient (Figure 3). Because of the resulting "zig-zag" *k*-space trajectory, and because only half of *k*-space was covered in these early implementations, images produced from a single excitation were not useful but nevertheless tremendously promising and exciting. The problems resulting from the sampling of only one half of *k*-space become increasingly severe as the field strength is increased. In 1987 Mansfield's group (20) introduced the FLEET (Fast Low angle Excitation Echo-planar Technique) and BEST (Blipped Echo-planar Single-pulse Technique) methods that solve the reconstruction problems by acquiring two images, one for the positive and one for the negative halves of k-phase. Using these techniques, and variants, Mansfield was able, by 1987, to collect complete MR images in as little as 100 msec. Since then they have shown high quality images of the head (21) and body (22) using the MBEST technology on their 0.5 Tesla research system.

2.4 Instascan Method Overview

The Instascan method, introduced in 1986 (23, 24, 25, 26), like echo planar imaging, utilizes rapidly oscillating gradients to spatially encode the MR signal. Instascan was developed between 1983 and 1986 to overcome the problems resulting from the larger, 2.0 T, static fields that were being used in imaging. Instascan differs from the EPI method in several respects. First, in the original Instascan presentation, all of the spatial encoding was performed under the RF-elicited Hahn spin echo (27). Second, pre-encoding pulses were applied along the phase and frequency encoding axes; as a consequence k-space is scanned symmetrically from -*k* to +*k* values. Finally, rather than leaving the phase-encoding gradient on continuously during acquisition, one gradient was pulsed briefly between each frequency encoding period. The result was a rectilinear, rather than a zig-zag, *k*-space trajectory; almost identical to the trajectory used in conventional imaging, though acquired in a small fraction of the total scan time.

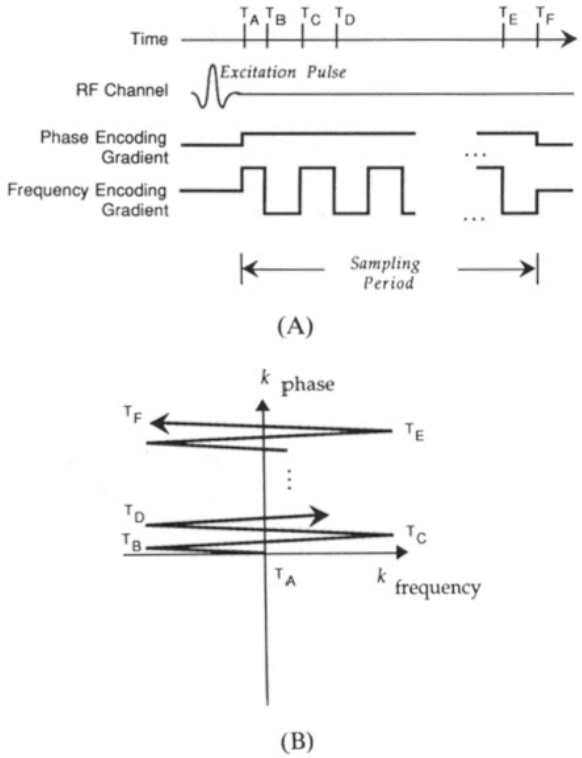

Fig. 3. (A) Pulse sequence used in the original echo-planar method. Following an RF signal excitation pulse the phase and frequency encoding gradients are applied simultaneously and the MR signal is continuously sampled. The polarity oef th frequency-encoding gradient is oscillated during data collection. (B) *K*-space representation of the echo-planar pulse sequence in (A). The MR signal traverses the spatial frequency plane in a zig-zag pattern as the polarity of the frequency encoding gradient is rapidly alternated. At time point T_A, there is no spatial encoding. By Time point T_B the combined effects of the frequency and phase encoding gradients result in a net positive displacement in both the phase and frequency directions. By T_F, the end of the encoding period, half of the *k-space* plane has been covered. While the points along the axis at *k*-frequency = 0 are evenly covered, as the displacement from *k*-frequency = 0 are increased, the spacing of the points becomes less regular. Several algorithms have been proposed to correct for this uneven spacing[13,28] but in practice[20] it is ordinarily desirable to use multiple excitations to compensate for the resulting phase errors.

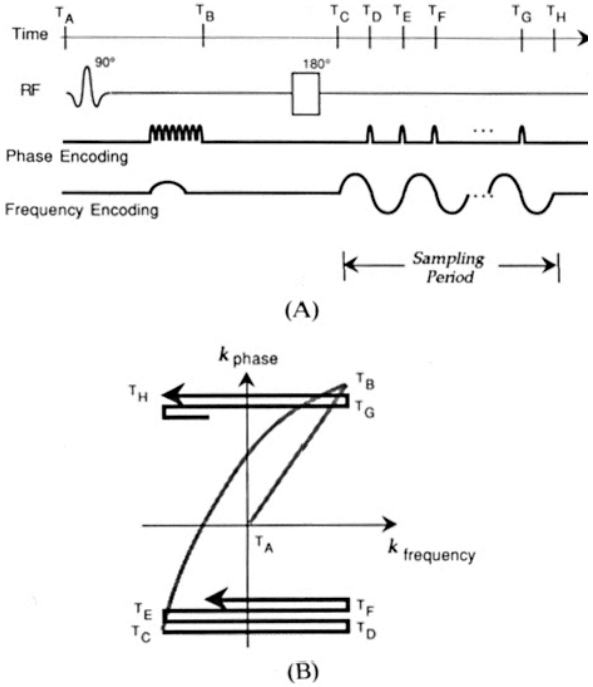

Fig. 4. (A) Instascan pulse sequence. In Instascan imaging, as originally proposed, all spatial encoding is performed on the RF spin-echo signal formed by a 90° and 180° RF pulses, and the encoding period is centered under the resulting spin-echo enveloped. The frequency-encoding gradient is rapidly alternated in polarity and the phase-encoding gradient is pulse briefly at each alternation point. A pre-encoding pulse is applied on each of the gradient channels prior to the sampling period. (B) *K*-space representation of the Instascan pulse sequence. Initially, at time T_A, the MR signal has no displacement on the k-space plane. The pre-encoding pulses, applied immediately after each excitation, give a net positive displacement on both axes by the time T_B and the 180° inversion pulse has the effect of displacing the signal to the opposite corner of *k*-space where sampling commences at time point T_C. Because only the frequency-encoding gradient is applied at this time, the trajectory in *k*-space is horizontal. Brief pulses of the phase encoding gradient at time T_D, T_E, etc… displace the signal upwards on the *k*-frequency axis. Overall the method results in a rectilinear traversal of *k*-space analogous to conventional MRI-encoding schemes, minimizing phase errors and image shape distortions.

2.4.1. *Instascan Pulse Sequence.* For the original Instascan studies, a 90° – 180° RF excitation scheme was used to produce both maximum signal, and, as described below, conventional contrast behavior. This pulse sequence is diagrammed in Figure 4A. As in conventional MRI, spatial information is encoded by the use of two gradient sets along orthogonal axes. Like its echo-planar relative, Instascan frequency encoding is performed with a rapidly alternating gradient. Originally a spatially selective 90° pulse was followed by a frequency-selective 180° pulse in order to provide the requisite chemical shift selectivity (cf. section 2.6.1 *"Chemical Shift"*), though later implementations have modified this scheme.

2.4.2 K-*space trajectory*. The consequences of using brief pulses of the phase encoding gradient are easier to understand in the context of the *k*-space representation (see Figure 4B). Because the phase- and frequency-encoding gradients are used alternately, rather than simultaneously, the trajectories along the frequency axis of *k*-space are flat, rather than tilted, and trace out a "raster-like" pattern. The raw data space is therefore covered more homogeneously, and the

image reconstruction process is similar to that of conventional imaging. The displacement in *k*-space along the frequency axis is determined by the duration and amplitude of the frequency-encoding gradient pulses while the total displacement along the *k*-phase axis is determined by the duration and amplitude of the phase encoding gradient pulses *and* by the total number of scan lines.

2.4.3 *Contrast Behavior*. Because the Instascan images are formed under the RF spin echo envelope, they have contrast behavior like that of conventional spin echo images (Figure 5 and Figure 6 (see also Figure 9)). Unlike the gradient echo methods (FLASH, GRASS, etc…) it is possible to use relatively long echo times to obtain true T_2 weighting. Furthermore, because the technique uses only a single excitation pulse, it is possible to obtain "infinite TR" images: scans whose contrast is independent of T_1. A common (though by no means universal) property of

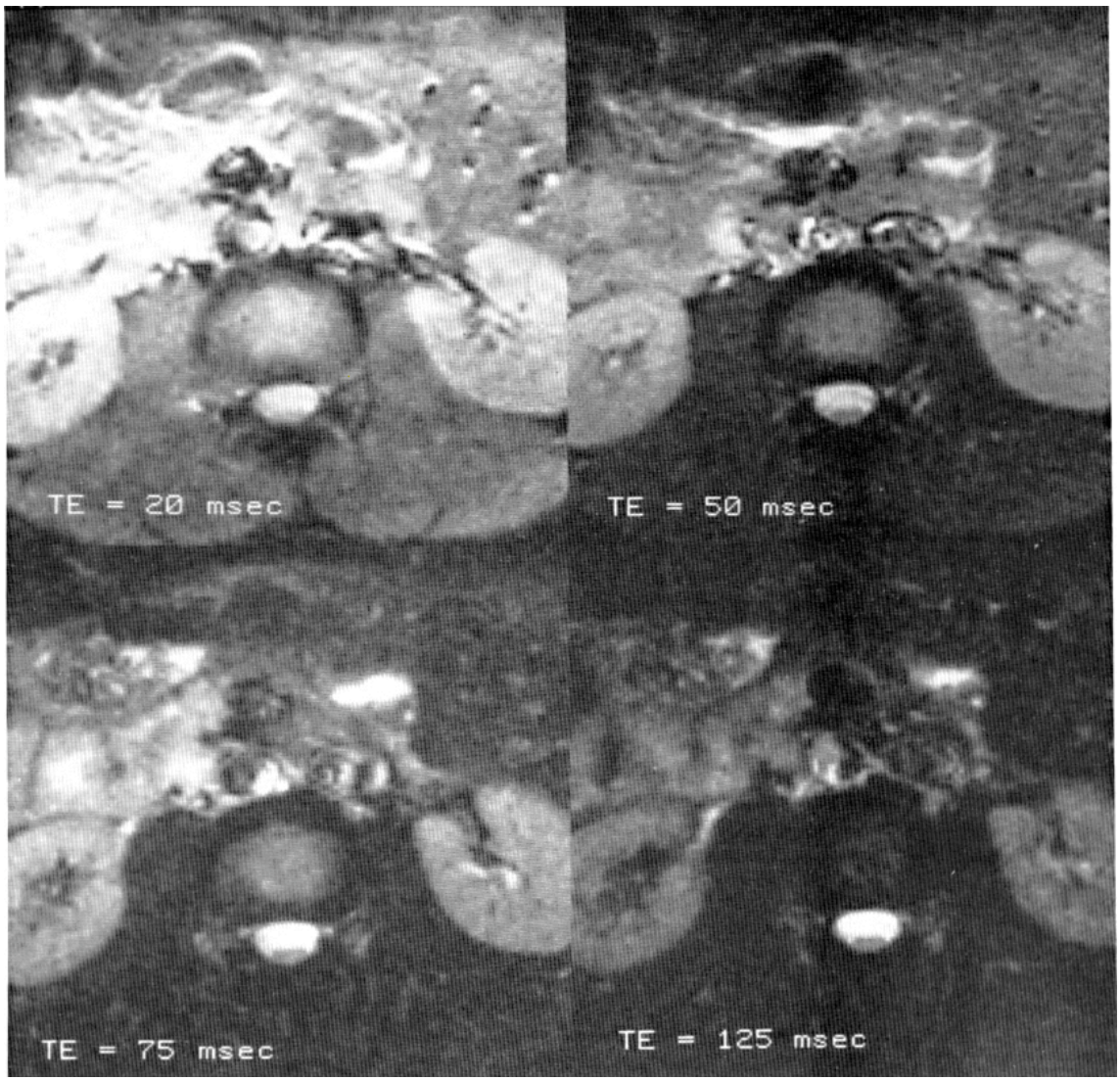

Fig. 5. Variations in abdominal image contrast as a function of echo time (TE). The above images were acquired using the partial *k* Mosaic Instascan method which requires two RF excitation pulses, separated by a TR period (see section 2.5.4 of the text for a description of the method). With TR kept at a constant 6 sec the TR of these scans was varied from 20 to 125 msec (as labeled on the images). Note, for example, the conspicuous decrease in muscle signal, relative to cerebrospinal fluid, as Te is increased. As a consequence of the very long TR, and due to the fact that the images are acquired under a Hahn spin echo, the signal intensity variations are dominated by T2 processes (as opposed to T2* or T1 effects). Grossly, the images are similar to conventionally acquired scans, though motion artifacts are reduced substantially. The pixel size (i.e., the spatial resolution) is 1.5 **x** 1.5 mm (128 **x** 128 matrix), slice thickness is 10 mm. The total scan time is simply the 6-sec TR delay between two successive RF pulses. Water only (fat-suppressed) images.

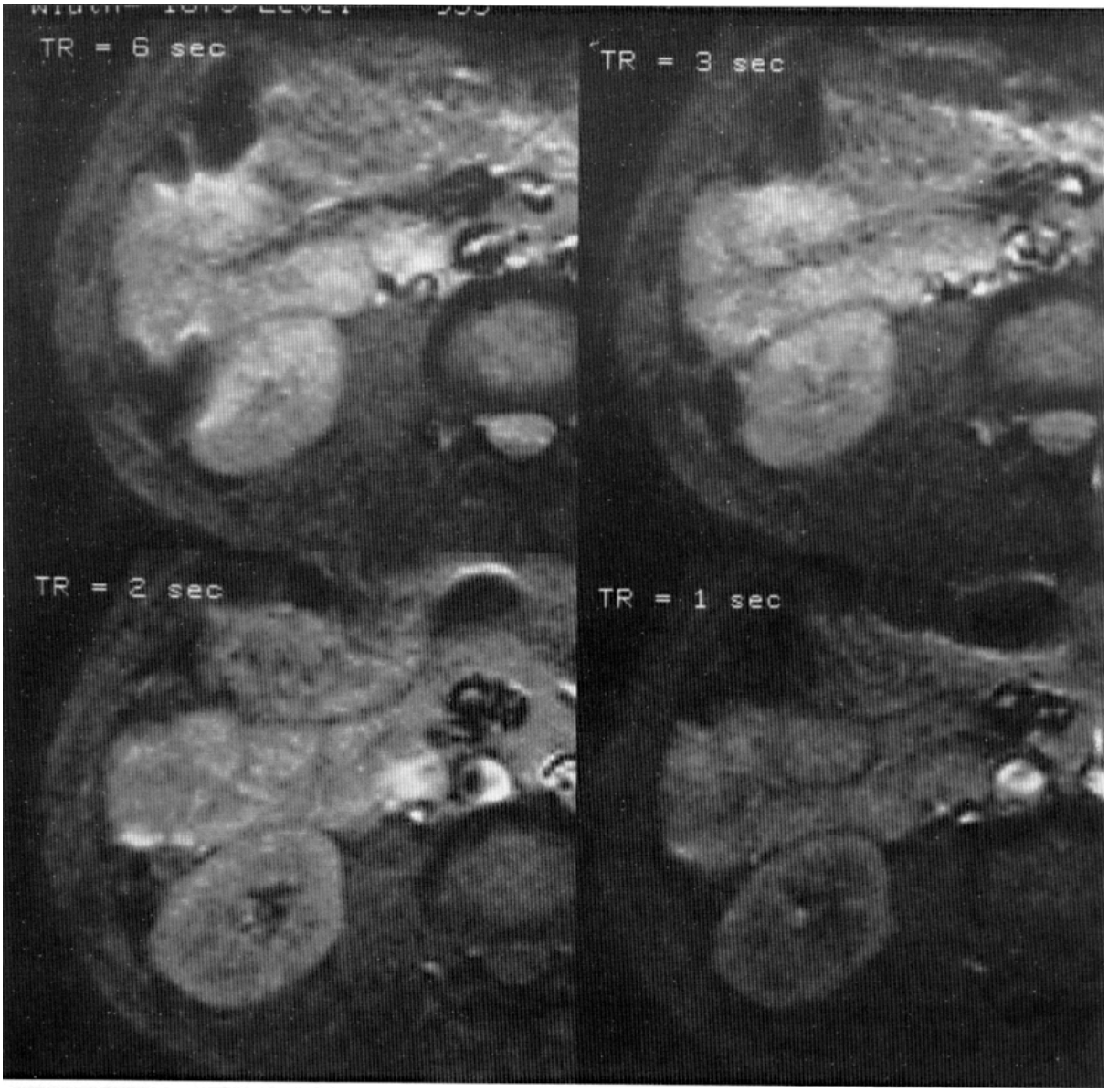

Fig. 6. Variations in Instascan image contrast as a function of TR. By varying the TR between two successive RF pulses used in acquiring each of these images, the T_1 contribution to image contrast can be varied. Except in the cerebral spinal fluid, little change in signal intensity is seen in the abcomen as TR is decreased from 6 to 3 sec. Further reduction in TR to 2 sec reduces the signal in the medulla of the kidney, the CSF and the intervetebral disk. With a 1 sec TR, good contrast is seen between the cortex and medulla of the kidney, but the signal is overall much reduced. Data were collected using the partial *k* Mosaic technique. The TE was kept constant at 26 msec. Slice thickness and spatial resolution as in Fig. 5.

biological tissues is the tendency for disease to be associated with simultaneous increases in both T_1 and T_2. In spin echo images the T_1 increase causes a signal loss while the T_2 increase results in a relative signal gain. As a consequence, lesion conspicuity is often compromised by residual T_1 contrast in T_2-weighted scans (or by residual T_2 contrast in T_1-weighted images); Instascan therefore offers the advantage of significantly improved diagnostic contrast behavior.

It is a straightforward matter to introduce any amount of T_1 contrast into the single-shot images: the image acquisition need merely be preceded by any additional RF pulse. In fact, the standard basis set of MR images: spin density-, T_2-, and T_1-weighted scans, can be acquired with only two excitatory RF pulses. After the first 90° pulse, two Instascan echoes at short and long TE are acquired, yielding the proton density and T_2-weighted contrast respectively, with an effective TR of infinity. A second 90° pulse is applied half a second or so later and a short TE Instascan image is acquired. This image will have T_1 contrast like that of a 500 msec TR conventional image. The overall imaging time

will therefore be only one-half second. Note therefore that in Instascan, paradoxically, the "long TR" (T_2-weighted) scans require less scan time than the short TR (T_1-weighted) scans. T_1 contrast may also be added by spin inversion, as will be discussed later (cf. section 2.5.1 *"Inversion Recovery"*, below).

2.4.4 *Gradient Strategies*. Performing all of the MR spatial encoding in only a few milliseconds requires strong and rapidly switched gradients. Looking once again to the *k*-space description, the spatial resolution along any axis is determined by the maximum displacement of the MR signal along the corresponding *k*- axis. This position is, in turn, determined by the integral of the applied gradient. If we wish to use brief gradient pulses, large gradient amplitudes must be applied to give the same overall integral. The large amplitudes require high current capability, and the rise time requirements place severe voltage demands on the gradient power sources. The prototype 2.0T Instascan device required gradients of about 4 Gauss/centimeter (40 milliTesla/meter) and had to reach these levels in about 150 μsec. In order to develop these gradient strengths, Rzedzian developed an energy efficient resonant gradient technology in which the inductive load of the imaging gradients is coupled to a capacitive network tuned to the desired operating frequency (27). By comparison, most of the current generation of imagers attain amplitudes of about 1 Gauss/cm in 0.5 to 1.0 msec. Changes to the specific *k*-space traversal pattern used in Instascan (see below) in its present configuration have reduced this requirement somewhat though the gradient requirements vastly exceed the capabilities of conventional gradient technology.

2.4.5 *Data Conversion Rates*. Not only must the gradients be rapid and powerful, but the image data must be collected extremely rapidly, requiring a wide receiver bandwidth, and fast analog-to-digital converters that must sample at nearly 500 kHz. The bandwidth in turn determines the SNR of the MR system. Generally, SNR varies inversely with the square-root of the receiver bandwidth: the wider bandwidth required for Instascan is therefore costly in SNR. As compared to conventional systems, the entire receiver chain, from the body RF coil to the audio filters must accept the increased bandwidth.

In Instascan, the alternating left-right trajectory through *k*-space requires a few additional steps in image reconstruction (27), the details of which are beyond the intended scope of this paper. (The interested reader may wish to consult the articles by Tropper (28), Twieg (13, 14) Bruder (29) and Schmitt (30) for more details.) For the Instascan device, where interactive imaging procedures are a major applications target, it is desirable that the image processing be as rapid as the data acquisition. Using specialized hardware and processing algorithms up to 5 images per second may be acquired, processed and displayed on the present system.

2.4.6 *Present Hardware Implementation*. The Instascan technology has been ported to otherwise conventional commercial imaging equipment. Presently, scanning is performed on a retrofitted General Electric Medical Systems Signa 1.5 Tesla scanner that is the source of all Instascan examples in this paper. Conversion of the Signa required extensive modifications to the gradients and RF probe, as well as the addition of high speed gradient power systems and appropriate control and image processing hardware. To enable the direct comparison of Instascan images with those acquired by other methods, the modifications has been designed so as to allow the changeover from conventional to ultra-fast operation in a few seconds. As compared the prototype 2.0 Tesla system, this implementation offers the advantages of wider patient access (identical to that of the conventional equipment) and full conventional imaging capability.

2.4.7 *Multi-Slice*. In conventional MR, data from additional slices can be obtained in the time between excitations of a given, single, slice. Therefore, collection of multiple slices takes virtually the same time as acquiring data from only a single slice. In the Instant methods there is often no repetition of the pulse sequence, and thus no TR (see Figure 7). As a result, the total scan time is increased with each extra slice. In practice the scan times are generally less than 1/10th of a second per image; the increased scan time in multi-slice is seldom a burden. Note also that if, for example, 30 slices are required, patient motion during the three second total exam time will not show up in the individual images, since each of these is acquired in only a few tens of milliseconds. Multi-slice acquisition is implemented in Instascan much as it is in conventional MRI: frequency-selective RF pulses are applied in the presence of a gradient to excite the tissue selectively at a given location in the magnetic field.

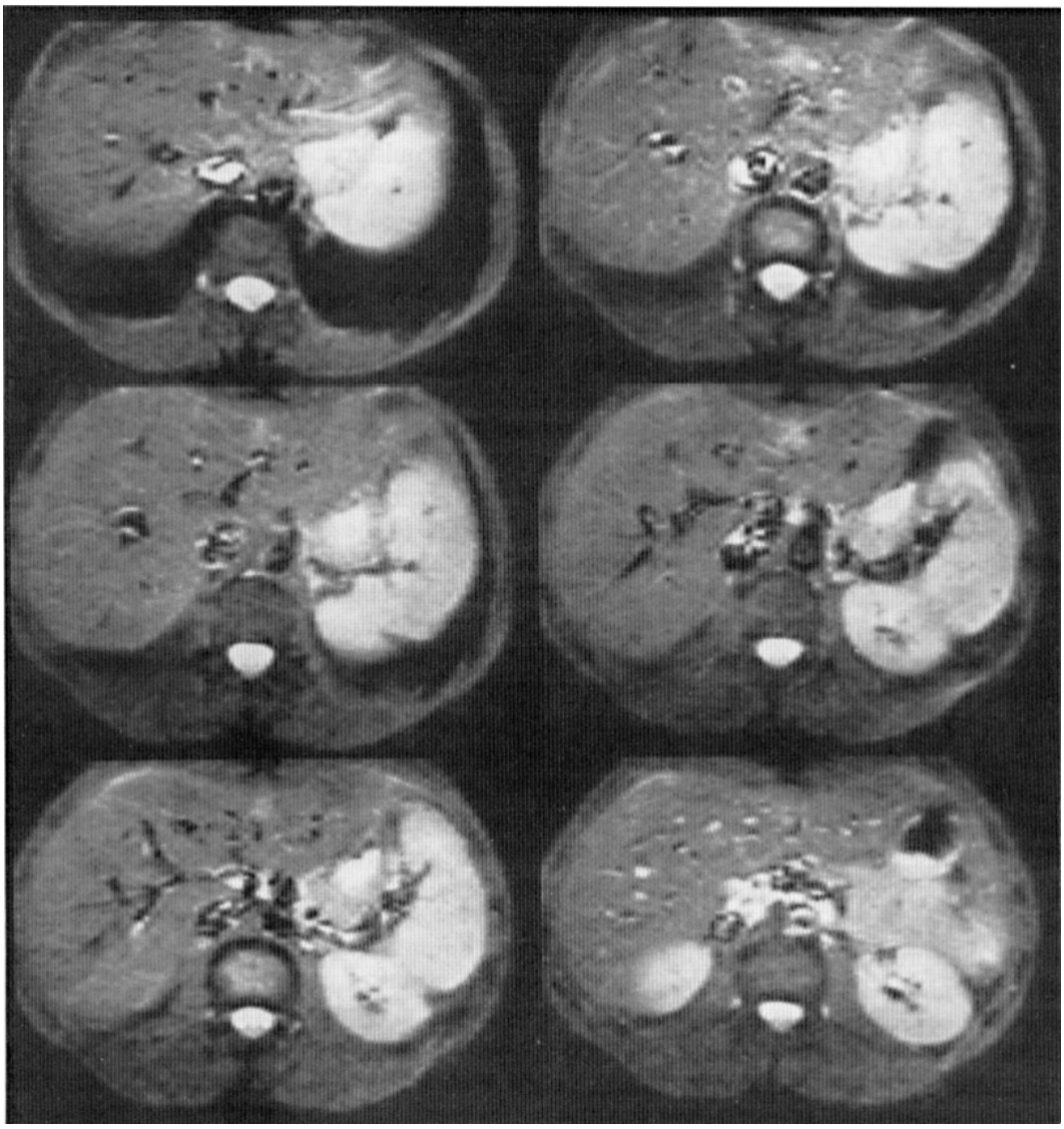

Fig. 7. Multislice, single-shot Instascan series. Because it is possible to obtain Instascan MR images with only a single excitation pulse, image contrast may be made independent of T1 as in these "infinite" TR scans. Each image was acquired in only 58 msec (so that the subject was able to breathe normally, and not special ecg or respiratory monitoring was required). The multislice examination, covering nine slice planes, was completed in 3 sec (though up to 32 slice planes could be imaged in that time). TE: 26 msec; slice thickness: 10 mm; spatial resolution 1.5 mm X 3 mm (128 X 256 matrix), water-only images

2.4.8 *Real-Time Mode.* The same principle used in gradient echo imaging, which allows rapid repeated excitations of a sample with little signal loss by using a shallow RF nutation pulse (cf. section 4.1.1 *"FLASH and Other Small Flip Angle Techniques"* below), can be applied to Instascan so that the same tissue slice may be imaged repeatedly with good SNR. When the repetition rate approaches the "flicker" rate of the eye (about 20 Hz) "Real-time" (31) images are produced. In the real-time mode it is practical to watch physiological processes as they occur. Even irregular motions of the heart and blood pool (32), for example, are followed easily. Practically speaking, real-time scans are among the easiest to acquire reliably. Cardiac movies may be collected without triggering, gating, retrospective ordering, respiratory compensation, or any other special setup. Furthermore, the real-time movies are resistant to changes in transmitter power (little, if any, prescan is required), and the patient has no responsibility to remain still during the exam.

The contrast behavior of the real-time Instant scans is similar to that seen in FLASH imaging. Increases in the flip angle result in increases in T_1 contrast, but generally at the cost of a loss in SNR. As flip angles are decreased, the images become increasingly proton-density weighted. On the typical real-time scan, stationary or smoothly flowing blood (see below) tends to be bright, as compared to the myocardium (32, 33).

2.5 Recent Developments in Instascan

2.5.1 Inversion Recovery. Preceding the Instascan sequence with a 180° RF pulse produces inversion recovery contrast (Figure 8). Such images have roughly twice the T_1 sensitivity of short TR (partial saturation) scans and are therefore useful in making highly T_1-weighted images (Figure 9). We often use the inversion recovery technique with an inversion time, or TI, (the time between the first 180° pulse and the 90° nutation pulse) corresponding to the time at which the magnetization of fat is at a minimum. With this inversion time (about 165 milliseconds) fat suppression is nearly complete, producing the Instant analog to "STIR" imaging (34, 35). Because this added contrast arises from a reduction in the signal from some tissues (as in most MRI methods) it comes at a cost in SNR. In practice some averaging is often used for inversion recovery imaging. A comparable method has been demonstrated in echo planar imaging using the MBEST technique which is similar to Instascan (36); preconditioning with an inversion pulse in high speed FLASH imaging has also been utilized to advantage (see below), but the resulting contrast behavior is different than that seen in conventional MRI.

2.5.2 *3D Volume Mode*. The 3D volume technique, as used in conventional systems, is effective in increasing the available SNR in contiguous, thin-slice images, at the cost, generally, of an increase in the minimum imaging time (37). It can be shown that where more than one excitation is required for acceptable SNR, and where the TR is approximately equal to the TE (as in gradient echo methods), the volume method offers a reduction in imaging time for coverage equivalent to multi-slice techniques. However, in conventional imagers the method is practical only for relatively short TR, because, unlike the multi-slice technique, the imaging time is multiplied by the final number of slices: collecting sixteen slices requires sixteen times as long (per NEX) as collection of a single slice. For this reason, volume imaging has been little used in spin echo MRI.

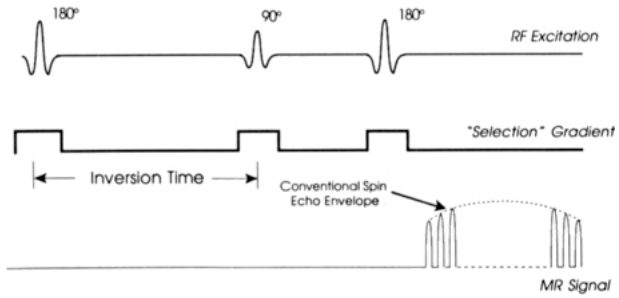

Fig. 8. Inversion recovery Instascan pulses sequence. Preceding the standard spin-echo Instascan pulse sequence with a 180° (inversion) pulse results in typical inversion recovery contrast behavior. The latency form the first 180° pulse to the excitatory 90° pulse is the inversion time, or TI.

We have explored the utility of volume methods in Instascan (38). Using a modified Instascan pulse sequence that includes an additional phase encoding step on the slice selection gradient (Figure 10), we are able to achieve good SNR on even very thin slices. While the method requires repeated excitations (in general as many excitations as slices) it is still possible to collect as many as sixteen thin slices, at long TR, in a single 48 second breath hold (with a healthy individual), as in figure 11. We have thus far used the 3D technique in the abdomen and heart, where 2 to 3 mm slice thicknesses obtained are otherwise difficult to achieve with either single-shot Instascan or with conventional imaging. Generally, the tissue volumes sampled simultaneously are larger in the 3D than in the 2D methods. For this reason the overall signal level is higher and a greater dynamic range is required from the analog-to-digital convertors in order to achieve the full theoretical advantage in improved SNR. When combined with the "real-time" mode (see section 2.4.8), 3D Instascan a sixteen partition scan can be performed in less than 1 second, making it a viable strategy for kinematic studies of joint motion (39).

2.5.3 *Resolution Improvements*. To understand better the spatial resolution limitations in MR imaging in general, and in the Instascan method in particular, we turn once again to the *k*-space formalism. Recall that points near the origin of *k*-space correspond to larger spatial frequencies (larger image features) and that the relative size of the feature represented decreases with displacement along either the phase or frequency axis. In Instascan rapidly switched gradients are utilized to trace out a path in *k*-space covering a limited area (Figure 12A). Simply making the gradients stronger and faster is not necessarily possible due to physical limitations of the gradient power systems (40, 41, 42) and to U.S. federal safety regulations prohibiting the use of gradient fields that change at extremely high rates and amplitudes.

The coverage in *k*-space along the phase-encoding axis can be extended readily by acquiring more raw data lines. This, in turn, is done by increasing the total duration of the readout period. Doubling the duration of the encoding therefore results in a two-fold reduc-

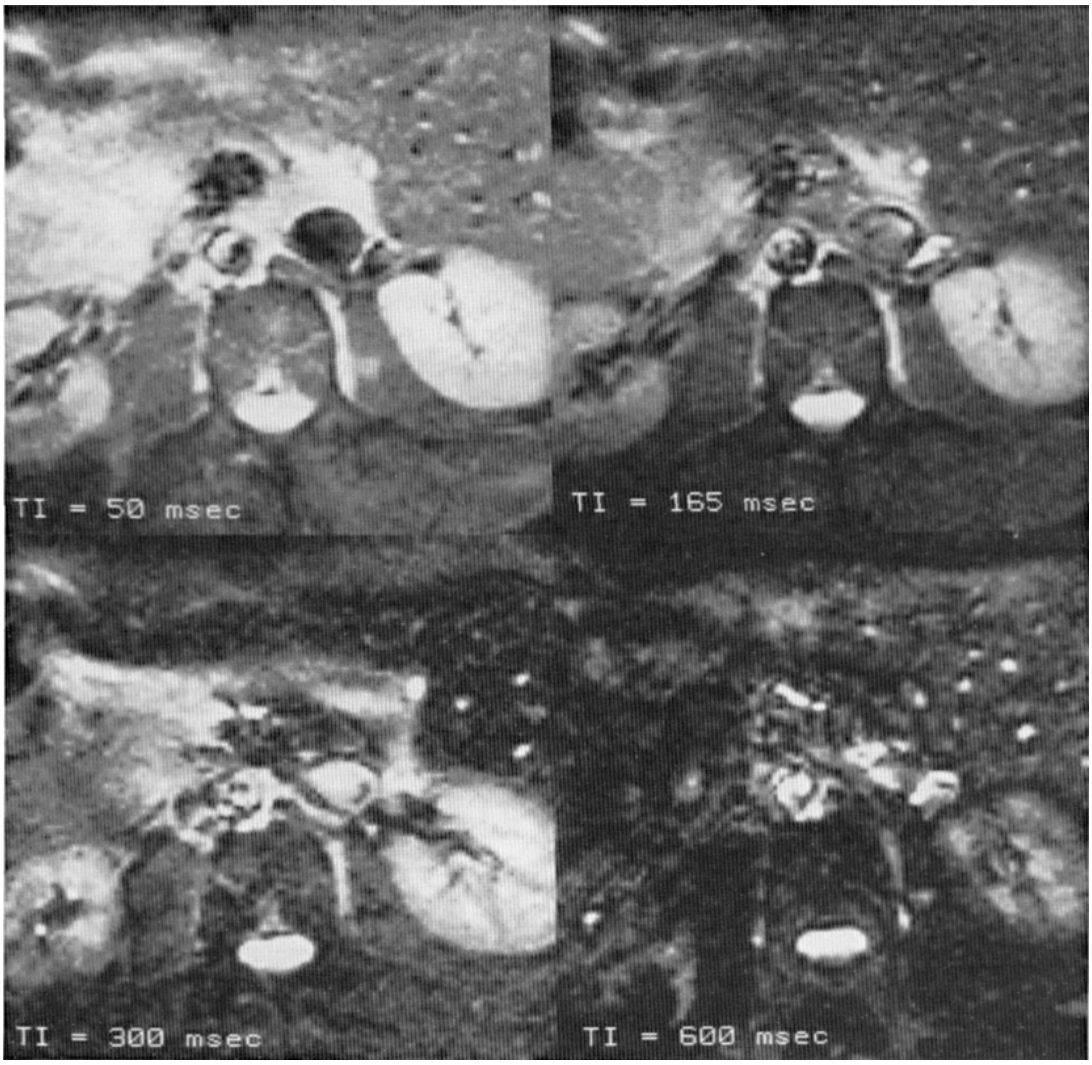

Fig. 9. Variations in inversion recovery Instascan image contrast as a function of inversion time (TI). The TI strongly affects the T1 contrast in the images. Note for example, in these abdominal images, the inversion in contrast between the cortex and medulla of the kidney as TI is increased from 300 to 600 msec. The near complete absence of signal in the liver at the inversion time or 300 msec indicates a T1 for that organ in the neighborhood of 200 msec. Because the T1 of muscle is much longer, its signal null occurs at about 600 msec. Since each of these scans requires only one Tr period, or 6 sec in this partial *k* Mosaic example (see section 2.5.4. of the text for a description of the method), it is practical to vary the TI over a broad range to maximize lesion or other feature conspicuity. TE: 26 msec; TR: 6 sec; slice thickness 10 mm; spatial resolution: 1.5 X 3 mm (128 X 256 matrix). These images are not lipid suppressed.

tion in pixel size, from 3 mm × 3 mm to 1.5 mm × 3 mm. The SNR is proportional to the pixel size; the two-fold reduction in SNR is offset somewhat by doubling the readout duration (in the full-*k* data set). This results in a combined SNR loss of only $\sqrt{2}$ for comparable TE. Generally, the Instascan pulse sequences have been designed such that the RF spin echo occurs at the center of *k*-space (at the center of the gradient echo) in the phase-encoding direction. With this scheme, extending the resolution along *k*-phase requires an increase in TE (Figure 12B).

2.5.3.1 *Control of Instascan Echo Time.* To offset the TE penalty, the conjugate symmetry properties of *k*-space may be exploited. To do so, the acquisition is started "off-center" in *k*-space by using a smaller amount of preencoding along *k*-phase; the portions of *k*-space not explicitly acquired are then calculated by the method of conjugate synthesis (17, 43) (Figure 13A and 13B) resulting in a doubling of final resolution with no burden in TE or total imaging time. This method is called "partial k Instascan". The same method has enabled the use of very short echo times (less than 10 msec on spin echo Instascan) as only a few lines of data need be acquired prior to the RF echo. In the partial-*k* implementation the SNR loss is easily offset by the possibility of dramatically reduced TE.

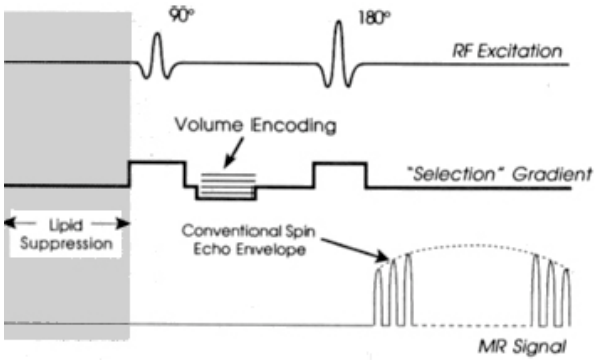

Fig. 10. Volume, or 3D, Instascan pulse sequence. The pulse sequences used for 2-dimensional and 3-dimensional Instascan differ only by the inclusion of a phase encoding gradient pulse on the slice selection axis prior to data collection. This gradient is used to separate the selected slice into partitions. While in the 2-dimensional method complete images are formed by a 2D fast Fourier transform following each RF excitation, 3D Instascan requires repeated excitations before the images can be reconstructed, using a 3D Fourier transform. In general, as many excitations are required as partitions. Because the signal following each excitations is correlated (since the entire volume is sampled with each excitation) the signal to noise ratio (SNR) achieved with the 3D technique is proportional to the square root of the number of partitions. This method therefore affords a substantial SNR gain, which can be utilized for thin slice imaging. An optional lipid suppression period precedes each sequence. For clarity, on the RF and selection gradient channels are shown, as the readout- and phase-encoding are identical to that used in the 2D sequence.

Figure 14 compares standard and extended resolution single-shot images.

2.5.3.2 *Mosaic.* Increasing resolution along the frequency-encoding axis is somewhat more difficult, as the present implementation of the Instascan device is limited by its resonant power system to a constant readout period; the *k*-space traversal with each gradient oscillation is therefore fixed. In the "Mosaic" technique, Rzedzian (44) used a tiling scheme to separately acquire data from different, but overlapping, regions of *k*-space following each of four separate Instascan acquisitions (Figure 15). Because it requires repeated acquisitions the technique is slow compared to single-shot Instascan. The total acquisition time was just over three times the intershot duration. The contrast in such images is determined by this intershot ("TR") period. In general, if a TR short than a few seconds is required it will be necessary to take one or more additional acquisitions in order to bring the magnetization of the sample into magnetic equilibrium. The technique may nevertheless be extended to achieve near arbitrary resolutions. In the original implementation the four excitations result in a four fold reduction in voxel size that is partially offset by the increased number of samples. Since SNR scales as the square root of the number of excitations, the SNR of the Mosaic scan is only $\sqrt{2}$ less than that of the single-shot image.

Weisskoff *et al* (45) have extended the partial-*k* technique to application along the frequency-encoding axis, combined with an extended readout period. These so called "partial read" images are single-shot images that yield a 1.5 mm × 1.5 mm in-plane image in less than 100 msec (Figure 16). Because the conjugate synthesis method may be applied only once, in this case along the frequency-encoding axis, the method has a relatively long minimum TE of 73 msec in order to acquire the full 128 frequency lines. It is also possible to acquire both halves of *k*-space explicitly with extended resolution in *k*-phase. This two shot Mosaic technique yields a $\sqrt{2}$ SNR advantage over the single-shot technique (Figure 17). We have recently extended these methods by combining the Mosaic and partial-k methods to yield high resolution at short TE. In this "partial Mosaic" method, two separate acquisitions are made, one with positive, and one with negative k-read values (Figure 18). Most the points, however, are collected on only the positive k-phase half plane, allowing the use of short TE's; conjugate synthesis is used to form the other half plane for a final image resolution equivalent to the four shot Mosaic technique in only two shots. Only one TR period, between the two excitations, is involved. The total acquisition time is therefore one third that of the original Mosaic, and the SNR remains high due to the short TE capability. Figures 5, 6 and 9 were acquired with this technique. A final extension combines the Mosaic and partial read techniques. The partial-read Mosaic technique, diagrammed in Figure 19 extends the resolution in the frequency-encoding axis by the Mosaic method and extends the resolution in the phase encode axis by extending the readout duration. With two shots it is therefore possible to achieve 0.75 × 1.5 mm in-plane resolution, as in the brain images shown in figure 20. By comparison, this is the same resolution achieved with a 20 cm field of view and a 128 × 256 matrix in conventional scanning.

2.5.3.3 *Other Multiple-Excitation Strategies.* A related technique, known as MESH (*M*osaicked *E*cho *S*can *H*ybrid), was also proposed by Rzedzian (44). With MESH, the amplitude of each pulse of the phase encoding gradient (and therefore the step between each data line along the *k*-phase axis) is doubled. Two separate acquisitions are used with the second set inter-

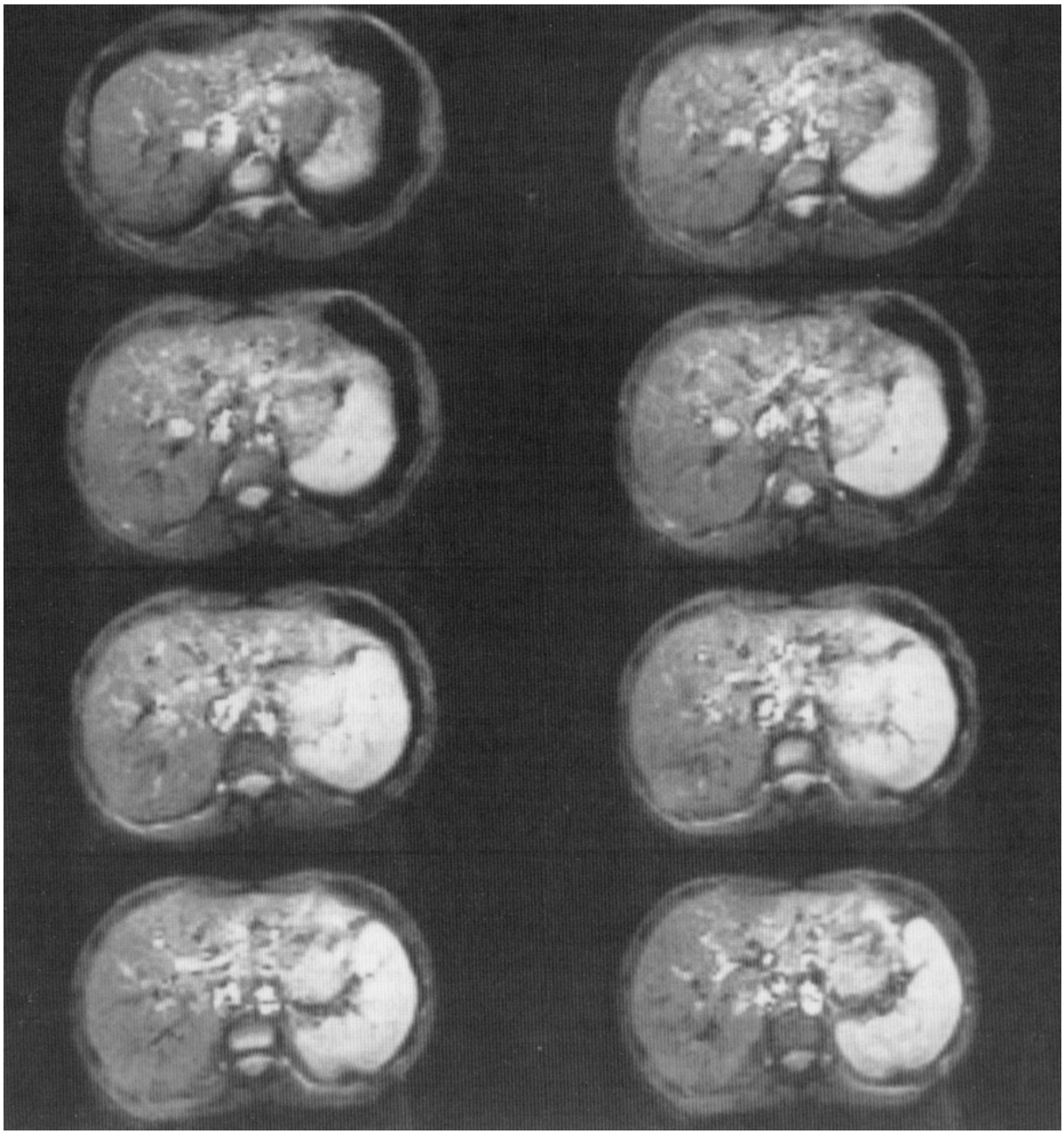

Fig. 11. Volume, or 3D, Instascan images. Using the 3D technique described in Fig. 10 with a 3-sec TR and a 42 msec TE, 16 3D partitions are obtained in 48 (16 X 3) seconds, a reasonable breath hold for a healthy individual. Because SNR is improved by a factor of four relative to 2D Instascan, it is possible to obtain very thin slices, as in these eight contiguous 3-mm sections (from the 16-slice image set).

leaved in the spaces between the data lines from the first set (Figure 21). An analogous method has been applied by others (46) to implement echo-planar-type imaging on a wholly conventional scanner.

The generalized issue of improving spatial resolution by the combination of separately acquired Instascan shots is a fertile area for research as questions still exist on the sensitivity to flow, limiting resolution, line broadening from T_2 and T_2* and a host of other issues. These multi-shot methods tend to fill in the presently existing gap between conventional and instant imaging approaches. In clinical practice, operating points will be defined that appropriately trade off SNR, resolution and motion sensitivity.

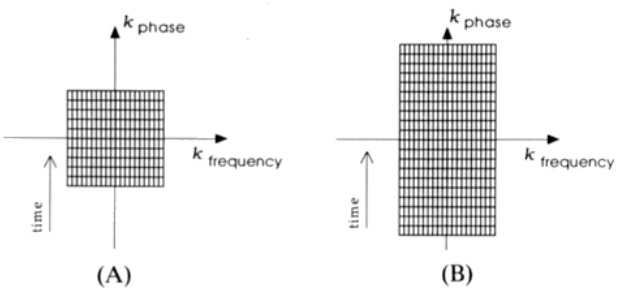

Fig. 12. *K*-space representation of standard and extended resolution Instascan. (A) Standard resolution. In Fourier transform imaging, the coverage of the k-space plane determines the spatial resolution of the final image (see Fig. 2 and section 2.2.1 of the text for a more detailed explanation). In single-shot approaches, such as Instascan, one factor in determining the extend of k-space coverage is the total time spent encoding the MR signal, which must be short compared to the transverse (T2) relaxation time in order to produce images with reasonable contrast behavior and relative freedom from artifacts. Recalling the k-space trajectory diagrammed in Fig. 4(A), Figure 12(A) shows schematically the k-space area which can be covered in a single 32-msec period in Instascan resulting in 3-mm in-plane resolution. Because k-space is sampled anisotropically, the field-of-view of the image will be oblong. (B) Extended resolution. By doubling the time spent in spatial encoding (by extending the readout oscillating portion of the pulse sequence shown in Fig. 4A) the extend of encoding along the k-space (vertical) axis is doubled. The final image will have anisotropic spatial resolution: 1.5 mm X 3 mm in-plane. The requirement to center the Hahn echo in k-space, however, demands that the minimum TE be extended, in this case to 73 msec.

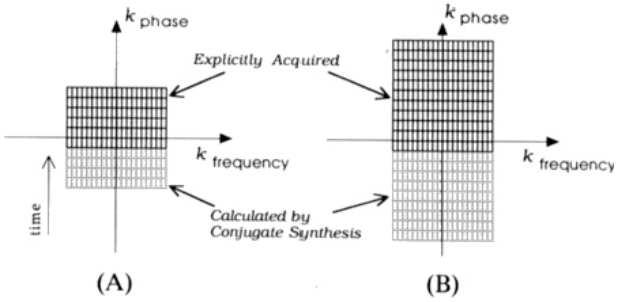

Fig. 13. Use of conjugate synthesis to reduce TE in Instascan. (A) Standard resolution. In single-shot methods, the minimum TE may be reduced by taking advantage of the conjugate symmetry of k-space. In this scheme, only slightly more than half of k-space is acquired explicitly (solid lines), with the Hahn spin echo centered in k-space only a few milliseconds after beginning the spatial encoding process. A variation of the, by now common, method of conjugate synthesis is used to calculate the remaining k-space half plane. A 3-mm final in-plane image resolution is obtained in 20 msec of spatial encoding – just over half of the time used in the symmetric trajectory shown in Fig. 12 (A). The minimum TE may be reduced to 20 msec or less in this manner. (B) Extended resolution. The conjugate synthesis method is equally applicable to the extended resolution scan. Note that the minimum TE is unaffected by the increase in resolution. Note that this technique is ultimately limiated, however, by the T2 of the sample; if the MR signal has decayed by the end of the encoding process, information about the high spatial frequencies (small image features) will be lost

2.6 Instascan Limitations

2.6.1 *Chemical Shift.* Chemical shift artifacts appear in MR images when the frequency differences between pixels are smaller than the intrinsic differences in resonance frequencies between chemical species such as water and fat. The result is typically a spatial displacement of fatty structures compared to aqueous tissues. In Instascan, each line of 128 raw data points is acquired in 500 μsec or less, so that the nominal bandwidth per pixel is approximately 2 kHz. Because this bandwidth far exceeds the nominal fat/water shift of 225 Hz (at 1.5 Tesla) there is no chemical shift apparent in the images along the frequency-encoding axis. However, along the phase encode axis (in the columns of data as represented in figure 4B), the time between successive raw data points is 500 μsec, and thus the total readout duration of 32 msec gives an effective bandwidth *per pixel* along this axis of only 30 Hz. As a result, the chemical shift artifacts in uncorrected Instascan images can be quite severe, extending for approximately eight pixels in the phase encoding direction (a spatial shift of about one-eighth of the image). Similar considerations require correction of images from other single-shot imaging methods such as square-spiral imaging (42, 47) and echo planar imaging (18).

A variety of solutions have been implemented to eliminate chemical shift artifacts in instant imaging by suppression of either lipid or fat signals. In a departure from the traditional binomial hard pulse series of Hore (48), Weisskoff (35, 49) has developed a hard pulse series designed to selectively excite, and subsequently crush, the lipid resonance over a fairly wide frequency band while only minimally affecting the water signal. This "optimally flat" +1 +4 –10 +4 +1 hard pulse series has practical advantage over the more familiar binomial series in that fat signal is more uniformly suppressed in the presence of magnetic field inhomogeneity. Alternatively, Instascan images are sometimes acquired using inversion recovery (STIR) methods for fat signal suppression as described below (35). While the STIR method is extremely robust, the added T_1 contrast, or corresponding SNR loss, from the technique is at times undesirable. Finally, more traditional frequency-tailored soft pulses may be used. Depending on the application, any of these solutions may be effective in suppressing lipid signal to below the noise.

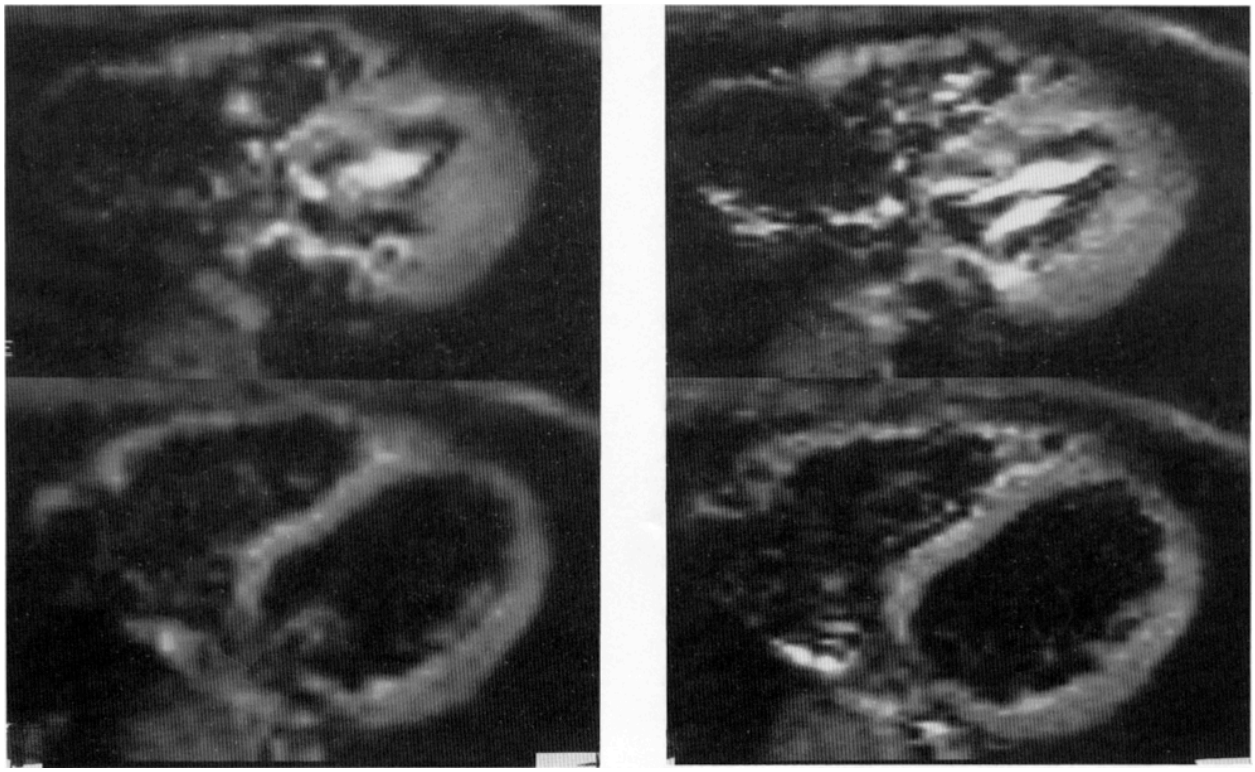

(A) **(B)**

Fig 14. Comparison of standard and extended resolution single-shot images. Figure (A) shows a pair of standard resolution (64 **X** 128) Instascan cardiac images with 3-mm in-plane resolution while (B) shows extended resolution (128 **X** 128 matrix 1.5 mm **X** 3 mm in-plane resolution) scans. Notice the improved conspicuity of small features in (B). TR: ∞; TE: 26 msec; slice thickness: 10 mm; total acquisition time for (A) is 42 msec and for (B) the acquisition time is 66 msec.

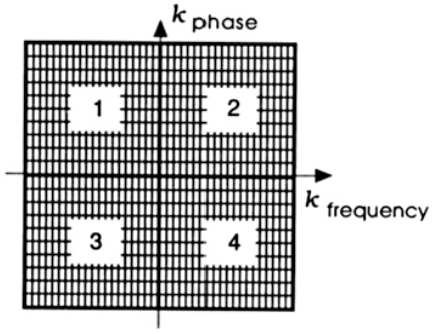

Fig 15. "Mosaic" Instascan. In the Mosaic technique, the k-space plane is "tiled": two or more shots are used (in this example four shots are used), each covering a different section of k-space. These data sets are then concatenated and a 2D Fourier transform results in a high resolution image. In the figure, each numbered area bounded by a heavy border is acquired following a single excitation (shot). Generally, the areas are allowed to overlap slightly. The same area may be covered in k-space with two extended resolution shots, with the penalty of an increased minimum TE. See Fig. 17 for examples.

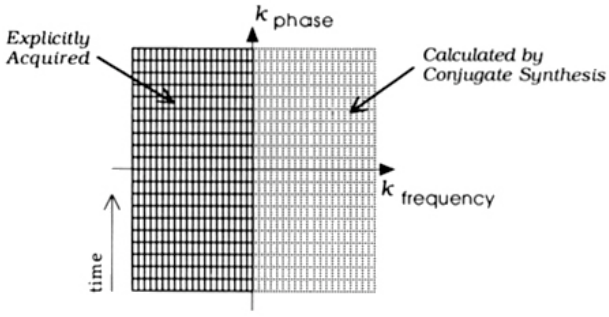

Fig 16. "Partial read" method. The conjugate synthesis technique may also be utilized in the readout direction to produce enhanced resolution along that axis. In a single-shot implementation, an extended resolution acquisition (Fig. 12(B)), displaced along the k-read axis, is used to acquire half of the k-space plane explicitly. The other half plane is calculated by conjugate synthesis. The final in-plane resolution is 1.5 mm **X** 1.5 mm. As in the scheme in Fig 12(B), this results in a relatively long minimum TE of 73 msec, but such scans are generally acceptable in the central nervous system (see Fig. 22 for an example) where tissue T_2's tend to be long. Because only a single excitation pulse is used, the total acquisition time is kept to just 1/10th of a second.

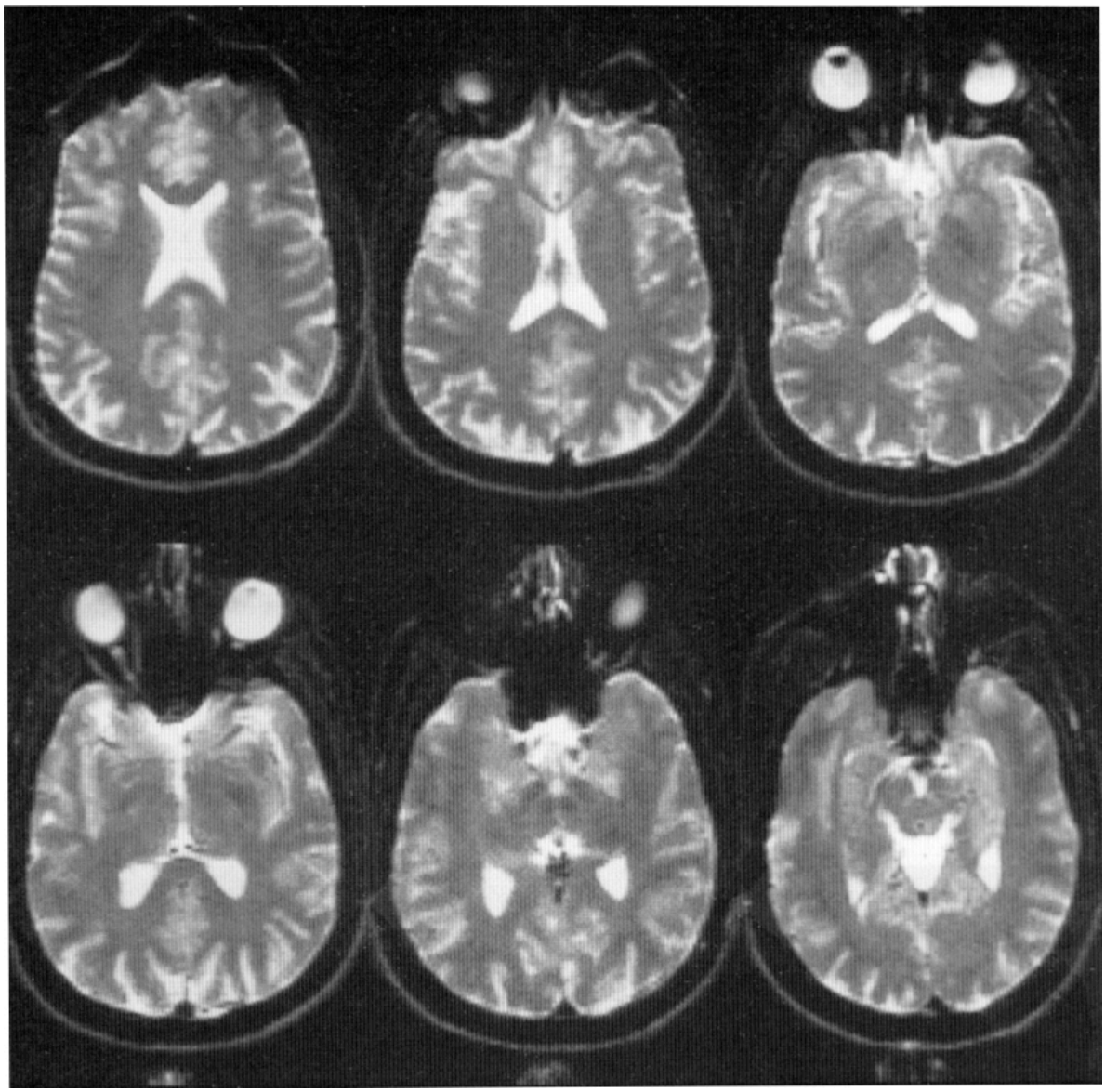

Fig. 17. T2-weighted brain images obtained with the two-shot Mosaic method. As compared to the partial read method (Fig. 16) the Mosaic technique affords an SNR improvement of more than 30%. One utilization of that increased SNR is to reduce the slice thickness, as in these 4-mm sections from a multislice two-shot Mosaic series. The total scan time for the series is just under two times the TR (for each image, it is one TR period) and up to 10 slice planes can be covered for each second of TR in multislice mode. TR: 5 sec; TE: 73 msec; slice thickness: 4 mm; spatial resolution: 1.5 mm x 1.5 mm (128 x 256 matrix). Note the very high T_2 contrast which results from the long TR and conventional T_2 weighting.

A novel method developed by Meyer *et al.* (50) utilizes crafted RF pulses to combine slice selection and frequency selection. Technologies such as these may become important in practical implementations of commercial instant imaging devices.

2.6.2 *SNR vs. Resolution*. Ultimately the goal of achieving Instascan's temporal resolution and reduced imaging time results in a set of tradeoffs. MRI being a technique that exploits extremely small signals, achievable signal-to-noise ratio is often a limiting factor. It is a convenient metaphor to consider SNR as a limited resource that can be used to purchase contrast resolution, temporal resolution, or spatial resolution – the major determinants of image quality. Due to the elimination of T_1-related signal changes, single-shot (or very long TR) images have a general advantage of improved SNR and T_2 contrast behavior. In Instascan, some spatial resolution is traded for temporal and contrast improvements. In many organ systems there is no actual loss in effective spatial resolution, because of the decreased motional distortion as described above.

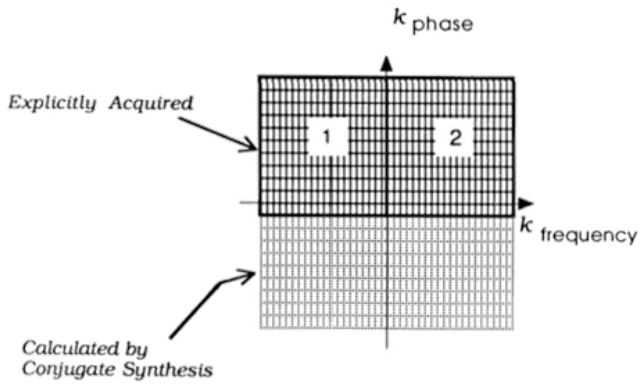

Fig. 18. Partial Mosaic *k*-space representation. In order to obtain high resolution in plane and short echo times, the conjugate synthesis and Mosaic methods may be combined. In this example, two shots are used to cover one half plane, each with a reduced TE. These data are then concatenated and the conjugate synthesis technique is used to calculate the remaining *k*-space half plane. Fourier transformation of the data results in images with 1.5 x 1.5 mm resolution in-plane like those shown in Figs. 5, 6, and 9.

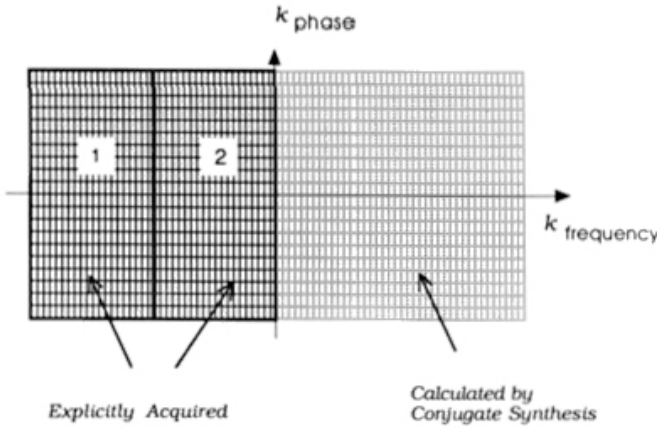

Fig. 19. Partial-read Mosaic scan technique. The combination of Mosaic and conjugate synthesis may also be used along the readout axis as diagrammed above. Here, the echo time is not reduced, but the spatial resolution in the readout direction is doubled. Two shots are acquired, both covering contiguous areas on one side of the half plane, quadrupling the resolution along this axis as compared to the "standard" Instascan method. Again, conjugate synthesis is used, and a final in-plane resolution of 1.5 x 0.8 mm is achieved in two shots.

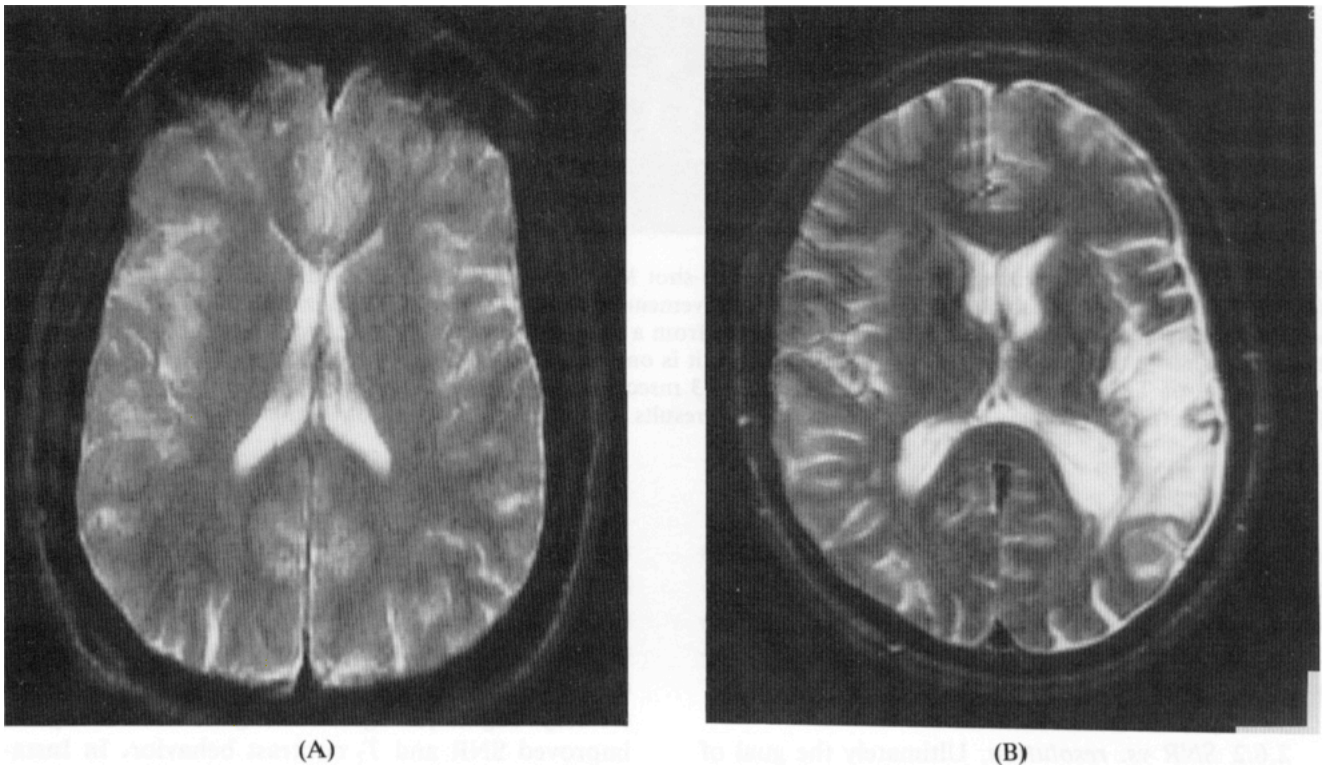

Fig. 20. Partial-read Mosaic image. (A) Images acquired with the partial-read Mosaic technique (Fig. 19) have a minimum TE of 73 msec and a total acquisition time of one TR period. The resulting in-plane resolution is 1.5 x 0.8 mm and excellent T_2 contrast is maintained. TR (and total acquisition time): 6 sec; TE: 73 msec; slice thickness: 10 mm. (B) For comparison, a conventional brain image from a different patient is shown. TR: 2.6 sec; TE 75 msec; slice thickness: 10 mm; total acquisition time: 10 min.

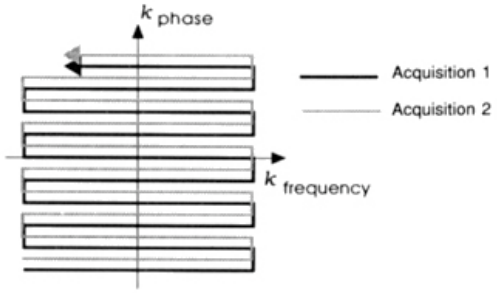

Fig. 21. Mosaicked echo scan hybrid (MESH) method. MESH is an alternative method for concatenating data from two separate shots. In this technique, the spacing between *k*-space lines is doubled for each of two acquisitions and the second scan is adjusted to cover data in *k*-read lines in the *k*-phase locations half way between those of the first acquisition.

In other cases, such as in the brain, improvements to MR image quality overall, through the use of quadrature head coils, improved RF pulses, and lower noise receivers, allow the acquisition of reasonably high spatial resolution Instascan images.

In our experience, the single excitation Instant images generally have adequate SNR for voxel volumes of about 15 mm^3 in the brain and with echo times as long as 75 msec. This is equivalent to a 7 mm slice thickness and a 1.5 × 1.5 mm in-plane resolution. When smaller voxel volumes are required, for thinner slices or for better resolution in-plane, we generally use a multiple excitation technique such as Mosaic, 3D or signal averaging for its SNR benefits. The T_2's of the abdominal organs, particularly the liver, are shorter than those of the central nervous system. Here, echo times of 30 msec or less result in good overall image quality. At the present time, our scanner is capable of acquiring images with 1.5 × 3 mm voxels at this TE with a single excitation, but even relatively thin slices are possible. As in any MRI technology, SNR in Instascan is determined both by measurement parameters, such as TR, TE, TI, slice thickness etc. and by the T_1, T_2, proton density and motion of the patient's body tissues. The final image quality therefore depends upon a careful match of measurement parameters to the clinical application. Fortunately, the image contrast behavior in Instascan is much like that of conventional MRI (Figure 22, and section 2.4.3 above) making predictions of contrast and SNR a straightforward task.

2.6.3 *Acoustic Noise*. The large, rapidly switched, gradient fields of the present implementation of Instascan produce relatively loud (100 – 110 dB) sound bursts, predominantly at 1 kHz, during the actual scan. Commercially available earplugs (e.g. E-A-R, from Cabot corporation, Indianapolis, IN) offer as much as 40 dB of acoustic attenuation at this frequency, so that there has thus far been no issue of patient acceptance. Even with earplugs, however, because the high speed protocols generally involve short imaging, separated by long quiet periods, the patients are occasionally startled by the scan. The short durations of the scans, however, have prevented this from affecting image quality significantly.

2.6.4 *Safety Issues*. Electrical currents induced in the body by time-varying magnetic fields are a cause for concern in the use of rapidly switched magnetic field gradients in MRI. The weight of considerable experience in conventional imaging supports the assumption of safety of the trapezoidal waveforms presently used in commercial devices. Reilly (51, 52) has reviewed the available data on excitatory thresholds for magnetic stimulation of the peripheral nerves and heart and has modeled these excitable systems in order to predict threshold behavior. According to these data, while the electrical thresholds for cardiac and peripheral stimulation are similar, the rate constants characterizing the excitable tissues of the heart are generally longer than those seen in neural tissues. As a consequence the predicted thresholds, measured in dB/dt (the rate of change of the magnetic field), for cardiac stimulation are much greater in the heart than in the peripheral nerves at the frequencies used for Instant imaging. Furthermore, the relatively small area subtended by the heart suggests that larger time-varying magnetic fields will be required for cardiac stimulation than for peripheral nerves (52). Bourland and his collaborators (53) have succeeded in generating extra-systoles in a dog via magnetic stimulation. At present, however, it is not clear how their stimulus paradigm compares with the exposures in MRI. In the course of safety testing of Advanced NMR's Instascan device, several experiments were performed on humans and animals at dB/dt levels, using transverse gradients considerably higher than those used for standard instant scanning. While no cardiac effects could be detected in either human or animal experiments, the volunteers reported that they occasionally felt marginal cutaneous responses (54, 55). Similar results were reported by Fischer *et al.* (56) using longitudinal gradients. Since that time, the Instascan instrument has been configured to oper-

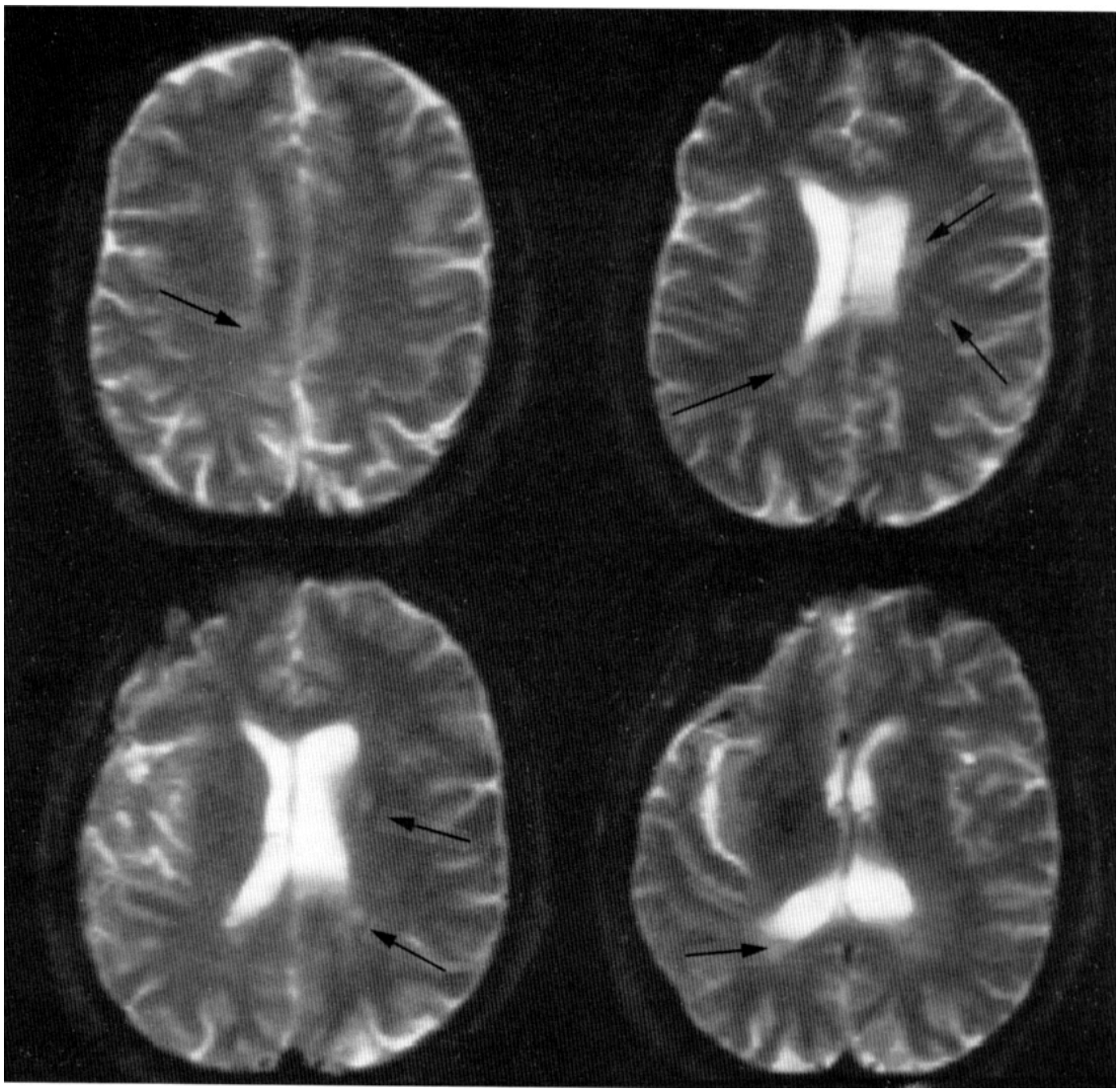

Fig. 22. Instascan brain images. These images, obtained using the "partial-read" method described in Fig. 16, demonstrate the conventional contrast behavior achievable with Instascan. Placques (arrows) resulting from multiple sclerosis are clearly visible and, because of the extremely strong T2 contrast, are readily distinguishable from the cerebrospinal fluid. TR: ∞; TE: 73 msec; slice thickness: 8 mm. Twenty-two images were obtained in six sec. of scanning.

ate within the much larger dB/dt guidelines established by the FDA. The practical acceptance of single-shot imaging clearly requires sufficient experience with the method to indicate its overall safety.

RF heating, quantified by the Specific Absorption Rate (SAR), has been a concern in conventional imaging sequences where the patient may be exposed to repeated RF pulses on a semi-continuous basis for the one hour or so required for a complete scan. The SAR for an imaging sequence is calculated as the average exposure during the scan TR period, regardless of the number of repetitions to which the patient is exposed. Generally the SAR for Instascan and real-time sequences is equal to or less than that used in conventional scans (since similar RF pulsing schemes are used). However, the total energy deposition (or dose) is typically much lower in instant imaging, as the exposure times are generally well under 10 seconds.

2.6.5 *Artifacts*. The unique sampling characteristics of single-shot imaging techniques, such as Instascan and echo-planar imaging, can lead to artifacts different than those seen in conventional imaging. Several major classes of artifacts are important: spatial distortion from T_2* (or T_2) decay, and from off-resonance effects; ghosting from inadequate control of gradient waveforms or sampling; and large chemical shift effects. Other artifacts, such as contrast aberrations from T_2 decay during sampling, or positional shifts secondary to velocity, are more subtle and may not noticeably affect the image appearance.

Some of the image distortions that can occur in instant imaging methods have been discussed recently by Farzaneh *et al.* (57) based upon assumptions as to the operational characteristics of the required imaging instruments. He has pointed out that spatial distortion artifacts, in particular, can be large when the total time for spatial encoding is long compared to signal decay times. When the encoding periods are long compared to the signal relaxation times (T_2*) the final spatial resolution may be compromised as well. Whereas short relaxation times result in line broadening in spectroscopy, in imaging the consequence will be a widening of the point spread function; that is a blurring of the image features.

In single-shot imaging the effective bandwidth may be quite low (see the discussion of chemical shift above) along the "phase-encoding" axis. Small deviations in resonance frequency may result in large displacements in the image. Like differences in chemical shift, local deviations in magnetic susceptibility cause frequency variations. In single-shot imaging methods, such as Instascan, this may result in shape distortions in certain regions, such as the orbits, where large susceptibility gradients occur. Schmitt (30) has presented a method for correction of some of the artifacts in instant imaging that result from resonance frequency variations. Such retrospective image correction is increasingly important as the readout duration is increased.

3. INSTASCAN APPLICATIONS

3.1 *Rapid Cranial Imaging*

In general clinical practice examinations of the central nervous system typically comprise 40 to 70% of the patient load. If Instascan affords a reduction in examination time for these patients, while maintaining uncompromised diagnostic image quality, it will have important beneficial impacts on both scan costs and patient acceptance of the MRI procedure. To this end considerable attention has been paid to improving the image quality of cranial images with Instascan (49, 58). While the comparative sensitivity of Instascan and conventional MRI in the detection of disease is still under investigation, preliminary studies (e.g. Figure 22) are encouraging and confirm that the overall contrast behavior follows that of conventional acquisitions. Using suitable instant imaging protocols the total examination time for complete brain studies will be well under one minute for a typical head screening. The insensitivity of ultra-fast imaging to patient motion should all but completely eliminate scan failures in uncooperative subjects.

3.2 Functional Imaging

Functional studies of the brain have proven utility (in PET, for example) in diagnosis of important diseases such as Alzheimer's-type dementia and in assessing the viability of tissue that may display no changes in signal intensity on standard MRI or CT scans (59). Although this dementia cannot yet be treated, the presence of a definitive diagnostic study can, as in multiple sclerosis, reduce substantially the number of otherwise unnecessary additional diagnostic procedures. In the absence of an effective *in vivo* diagnostic, candidate treatment methods can be assessed only by *post-mortem* study. The development of effective treatments is thus made extremely difficult. Many significant lesions, for example epileptic foci, are frequently invisible with even the best non-functional studies, yet it is reasonable to anticipate that the functional scan might allow us to find occult lesions. Both functional methods discussed below: dynamic analysis of contrast agent distribution and diffusion imaging, are designed to produce quantitative determination of regional perfusion. Tissue perfusion, in turn, may vary greatly with tissue health and, as has been demonstrated with PET scanning, brain functional activity.

3.3 *Susceptibility Contrast*

The first functional method we describe involves the observation of cerebral blood flow, by tracking the dynamic distribution of injected contrast agents. As a result of their large magnetic susceptibilities, paramagnetic lanthanide chelates, such as gadolinium diethylene triamine pentaacetic acid (Gd-DTPA) or dysprosium-DTPA (Dy-DTPA), when in high concentration in the bloodstream, produce large magnetic field gradients across vascular boundaries. When field echo methods are used for imaging, these induced gradients act to reduce T_2* relaxation times. As a consequence, the signal recovered in gradient echo imaging methods is reduced in the vicinity of the blood vessels when the concentration of contrast agent is high. The T_2 relaxation time is reduced also by locally high concentrations of paramagnetic contrast though the mechanism is somewhat different. Here the effect results from the loss of spin coherence as proton spins diffuse across the significant field gradients that exist at the margin of contrast agent-filled capillary spaces (60, 61, 62, 63). Therefore the dynamic properties of contrast agent perfusion may be evaluated, as well, from spin echo images.

The T_2 relaxation effect of Dy-DTPA was noted by Villringer *et al.* (60). Kantor has explored the potential of evaluating coronary stenotic disease and myocardial function by observing the time course of signal intensity changes after intravenous infusion of Dy-DTPA or Gd-DTPA. Using Instascan methods, cardiac images were acquired every one to two seconds following bolus injection of the contrast agent. In healthy dogs a transient signal intensity drop of about 20% (with Gd-DTPA) could be seen after a delay of about 12 seconds. Treatment with the vasodilator dipyridamole potentates this effect so that 80% drops in signal intensity were seen with a slightly earlier onset (64). In experimentally induced coronary stenoses, the dipyridamole-potentiated effect was seen to be significantly reduced distal to the stenosis (65, 66).

In the CNS, Belliveau and his coworkers have been examining the capabilities of Instascan to quantify cerebral perfusion. They have demonstrated that, in the brain, the transient signal attenuation produced by bolus injection of Dy-DTPA can be modulated by experimentally induced hypercapnia (67, 68, 69). The hypercapnia itself is known to be associated with cerebral blood flow, which increases linearly with pCO2 in the 20-80 mm Hg range. Variations in the Gd-DTPA effect have also been noted in experimentally induced cerebral ischemia (70). Using these methods they have produced quantitative maps of cerebral perfusion by integrating the signal intensity change on a regional basis (71). The technique has recently been reviewed by Rosen, Belliveau and Chien (63) and their work on human brain perfusion has recently been reported in another, more recent review (62). Analogous results are reported by Stehling (72) using the echo planar method. The FLASH method has been used as well (73) to evaluate contrast agent dynamics.

We can also anticipate that various mass lesions, such as tumors, may be better differentiated by their vascularity, adding specificity to the MR exam. This effect should show up both in quantitative flow studies and by the rate constants of approach to equilibrium concentrations of contrast agents. Future practical protocols may involve a contrast agent study that looks first at the susceptibility effects of the agents during the first 10 to 30 seconds following bolus gadolinium injection, and then examines the T_1 relaxation effects over the next few minutes as equilibrium distribution is reached.

3.4 Diffusion Weighting

More recently, the so-called Intravoxel Incoherent Motion (IVIM) method of Le Bihan (74) has been adapted for use in combination with a variety of single-shot imaging techniques. The original IVIM method uses spin echoes; after the method of Stejskal and Tanner (75), motion sensitizing gradients are added symmetrically about the 180° refocusing pulse. These gradients have the effect of dephasing the signal from diffusing spins, thus causing a signal loss on T_2-weighted scans. However, the large motion sensitizing gradients make the IVIM method extremely prone to motion artifacts in conventional implementations. Furthermore, *quantitation* of diffusion constants requires sampling the signal at a variety of diffusion sensitivities, each compromising a complete imaging sequence. The overall examination time is therefore too long for practical clinical scanning. In practice clinical utilization of the method has therefore awaited its incorporation into single-shot methods such as echo planar imaging (6) and Instascan (7). The EPI method was implemented in a 2T GE CSI imaging system equipped with 25 cm "Acustar" shielded gradient coils, while the Instascan implementation involved the incorporation of motion sensitizing gradients into the basic Instascan pulse sequence (Figure 23). Because the imaging times are kept extremely short compared to gross physiological motion – approximately 160 msec with Instascan and 94 msec with the small bore EPI method – the motion sensitivity is reduced dramatically. Within a certain range of motion-sensitizing gradient amplitudes the signal

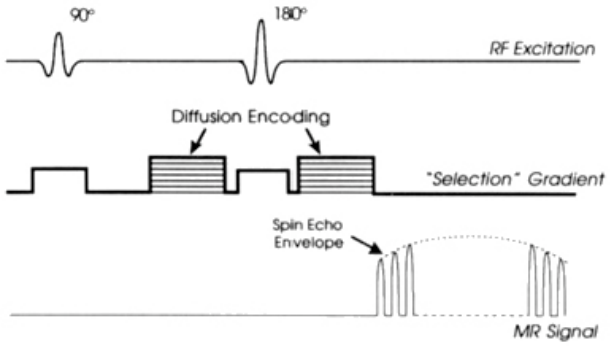

Fig. 23. Diffusion-weighted Instascan pulse sequence. Diffusion weighting is added to the Instascan imaging sequence by the application of large additional gradient pulses before and after the 180° RF pulse. These tend to strongly diphase any spins which change position over the course of the scan. Because these gradients are effective against any sort of motion, however, the method has only been practical in combination with single-shot techniques where motion effects can be minimized. The pulse sequence has been designed such that the amplitude of the diffusion sensitizing pulses may be automatically varied to cover a range of "b-values".

intensity loss is dominated by the effects of diffusion, while at lower amplitudes, perfusion is the dominant contributor to signal loss. From properly collected data, the modified IVIM method has the potential for the formation of regional perfusion maps without the use of contrast agents. Furthermore the diffusion itself offers an additional contrast factor that may be useful in disease and tissue differentiation.

3.5 Dynamic Motion Studies

3.5.1 *Heart*. Perhaps the most obvious applications of instant imaging are to the moving structures of the body, such as the heart, that are notoriously difficult to scan reliably via MRI methods. Such instant images were initially obtained by Rzedzian and Pykett (26) and showed the capability of the Instascan system to acquire freeze frame images of the heart without triggering or other synchronization timing. Subsequently, Drucker *et al.,* (76) validated the techniques in normal volunteers by demonstrating that measurements of thickening of the interventricular septum, left ventricle anterolateral wall and right ventricle were within the normal range.

Several methods for the acquisition of Instascan cardiac movies have been described (32). With spin echo acquisitions TR's of 2 seconds or more are used in order to reduce saturation effects. Cardiac movies are thus obtained by collecting a series of images, each at a different cardiac phase. The first method of forming such movies, termed pseudo-gating, involved setting the TR slightly longer than twice the average R-R interval (or integral number of R-R intervals). In this way, subsequent images were advanced slightly into the cardiac cycle. While this method has the advantage of rapid and simple setup, it was reliable only in individuals whose heart rate was constant over the 30 to 40 seconds required to collect the entire movie. Movies were also formed retrospectively from a time series of images acquired at a constant TR without special relation to the patient's heart rate. The images thus acquired were sorted according to their position within the cardiac cycle. A synchronized acquisition technique, called "progressive time delay" utilizes synchronization pulses from an ECG monitor. In this method subsequent images are electronically advanced following each R wave. Progressive time delay resulted in qualitatively smooth movies at the cost of a slight burden in setup of the ECG equipment and is the method of choice for the acquisition of spin echo Instascan cardiac movies (Figure 24). There is, theoretically, some contrast non-uniformity in the progressive time delay movies as a result of variations in the subject's heart rate. In practice, however, these effects are generally not visible. In all of these spin echo techniques, each image is formed during a fraction of a single heartbeat (as compared to conventional cardiac gated MRI in which each image is the composite of 128 or more heartbeats). The movie, however, is a composite formed from several heartbeats. In general, spin echo Instascan produces "black blood" cardiac images, though, at least without pre-saturation, the blood signal is somewhat variable.

The final cardiac movie technique described was real-time imaging (as discussed above). In this case the entire cardiac movies were acquired during a single heartbeat. Real-time imaging requires no cardiac synchronization and the quality of the movies is independent of variations in heart rate (Figure 25). Like the CINE technique (5) the real-time method is a "bright blood" protocol. The blood signal intensity is less homogeneous however, presumably as a consequence of un-averaged turbulence effects (33). The relative acquisition times are listed in Table 1.

3.5.2 *Gastrointestinal System*

3.5.2.1 Conventional Approaches In the gastrointestinal system, conventionally acquired MR images frequently are contaminated by artifacts due to patient motion (2, 77). A number of technologies have been developed to combat these problems in conventional MRI. Simple signal averaging may reduce the relative intensity of the motion artifacts (78) but will not remove them (79) and comes at a substantial penalty in either imaging time, or, if short TR's are used, in volume coverage. Respiratory gating, although at times fairly effective (80), also prolongs scan times significantly.

Because the dominant signals in much of abdominal imaging are from the lipids in the skin, the STIR technique can be fairly effective in reducing motion artifacts (34), and is clinically useful if the contrast behavior, set by the inversion time for fat, is diagnostically acceptable. Similarly, chemical shift selective presaturation methods (82, 83) may also be effective the re-

Table 1. Relative acquisition times for the collection of cardiac movies by MRI

Acquisition Mode	Heartbeats per 128 line image	Heartbeats per 16 frame movie
Conventional Spin Echo	128	2048
Instascan Spin Echo	1	16
Real-time Instascan	1/16	1

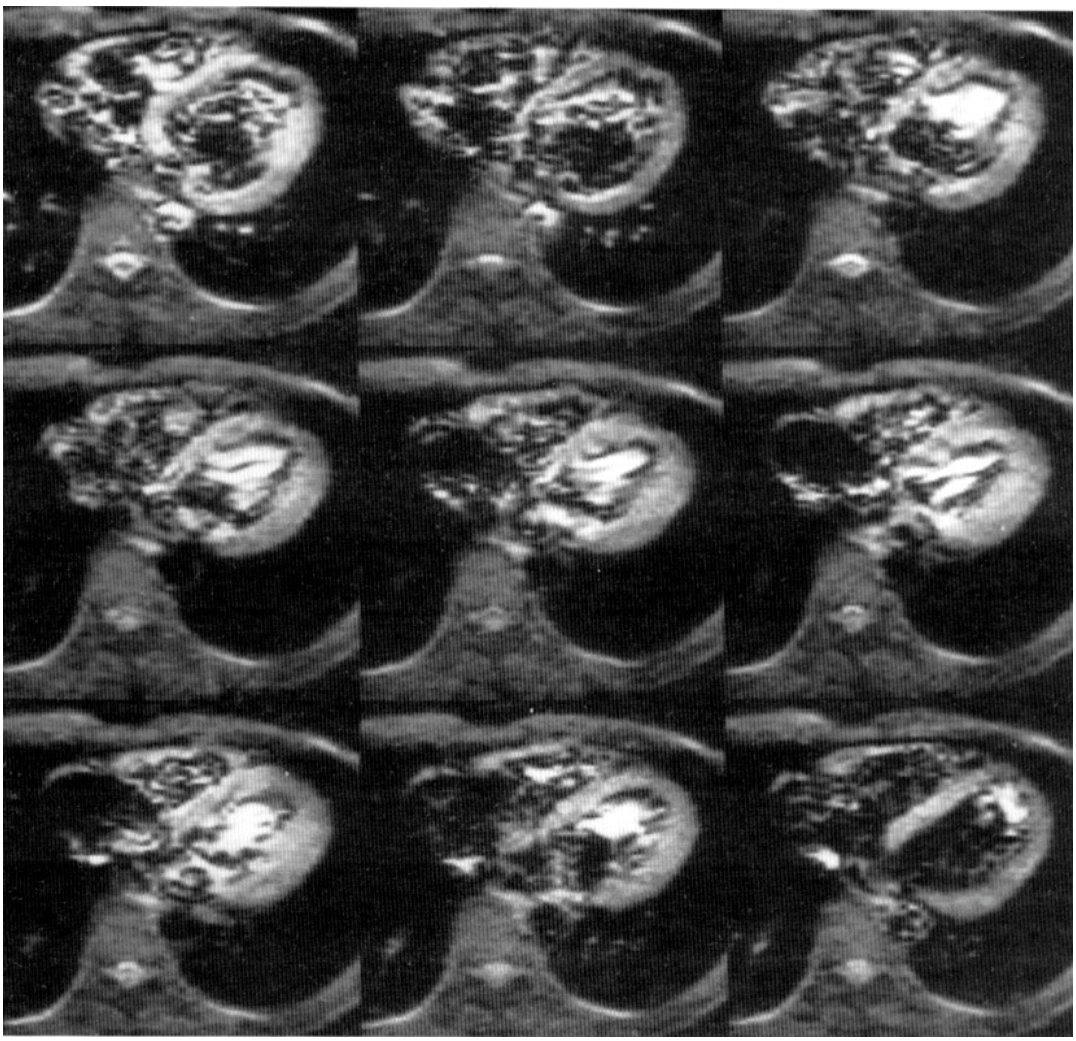

Fig. 24. Spin-echo cardiac movie. By incrementing the delay form the cardiac R-wave, prior to the collection of each of a series of cardiac images, a "movie" of the heart may be obtained. These scans, with 1.5 X 3 mm in-plane resolution, were each obtained in 56 msec during a single heartbeat. To minimize T1-related signal losses, one image was acquired with every other heartbeat, resulting in a total scan time of 40 sec for the 16 frame cardiac movie. TR: approximately 2.5 sec; TE 26 msec; slice thickness: 10 mm; 128 x 128 matrix.

duction of respiratory motion artifacts. The method known as respiratory ordered phase encoding or ROPE (84) minimizes artifacts by making patient motion a non-periodic function of phase encoding. ROPE and its relatives require careful monitoring of abdominal motion and may prolong scan time somewhat. Gradient moment nulling reduces ghosting from patient motion by ensuring that the phases of moving spins are not altered by their motion through the gradient fields (85) and has been used successfully to suppress some motion artifacts in abdominal imaging (79, 86).

3.5.2.2 *Ultra-Fast Methods*. Ultra-fast techniques are advantageous in the abdomen as they can frequently eliminate completely the artifacts from gastrointestinal and respiratory motion (72, 87). In their work with Instascan, Saini and his coworkers (88) also describe the elimination of motion artifact by the method as well as favorable T_2-dependent soft tissue contrast. These effects combined to allow them to detect even very small (5 mm) hepatic lesions. Stark (89) also reported favorable results in Instascan liver imaging.

3.6 *Rapid Time-Resolved Angiography*

Many methods presently exist for the collection of MR angiograms (see, for example, 90, 91, 92). A method for the rapid collection of time-resolved angiograms was recently developed (93, 94) that utilizes the unique capabilities of single-shot imaging. In this time-of-flight method, analogous to the single slice method used by Keller (95), real-time Instascan with flip angles of 90° or greater are used at short TR to saturate the magnetization of stationary tissue. In blood vessels, however, the in-flow of fresh

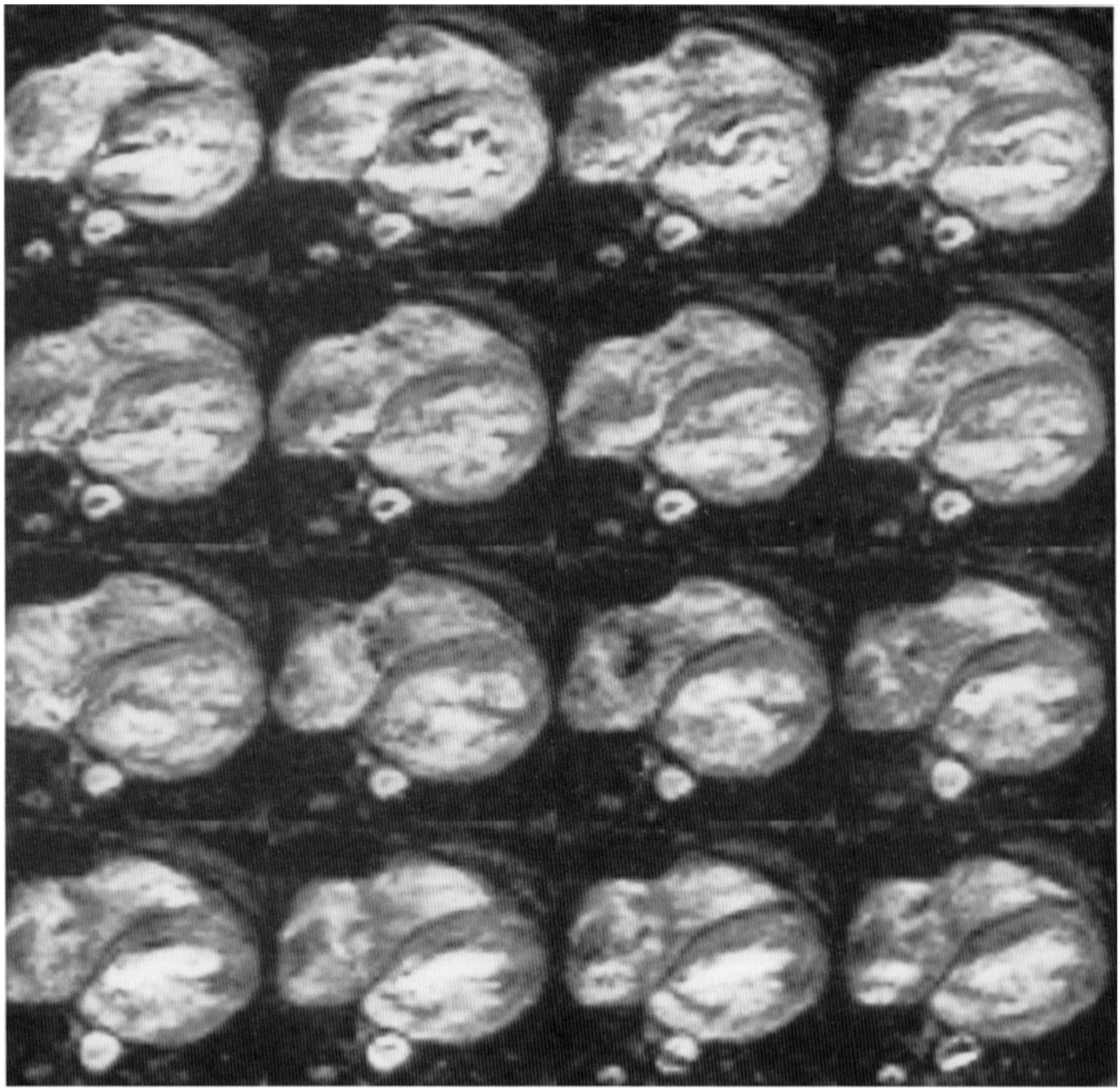

Fig. 25. "Real-time" cardiac movie. The "real-time" method, which utilizes reduced flip angles to minimize signal losses with repeated rapid acquisitions, results in images with contrast similar to conventional gradient echo techniques. This series of 16 images was obtained in a single heartbeat. Because such cardiac movies are not composites of multiple heartbeats, they show accurately the beat-to-beat variations in cardiac activity. TR: 67 msec; TE: 10 msec; slice thickness: 10 mm; flip angle: 30°.

spins to replace the saturated spins leads to a relatively large MR signal. Unlike other time-of-flight techniques, each excitation results in a complete MR image. Since many such images can be acquired in a single location over the course of a single cardiac cycle, it is possible, by tracking the electrocardiogram during acquisition, to sort the images retrospectively by temporal order. A series of such single slice movies are acquired over a large number of slices, and the maximum intensity projection ray-tracing method may be used to form these data into projection angiograms. Because the temporal order is preserved, these angiograms may be displayed as cine loops that show clearly the pulsatile flow in the large vessels of the body. In a typical protocol fifteen images are acquired at a TR of 80 to 100 msec at each of 39 locations. Generally the data collection is separated into three acquisitions each imaging thirteen locations. Since the data collection at all thirteen locations requires only about 16 seconds (15 images × 80 msec/image × 13 locations) abdominal studies can be readily performed with breath

holding. These studies are still preliminary, but their future applications to rapid dynamic vascular imaging in the abdomen and periphery are very exciting.

3.7 Interventional Uses of Ultra-Fast Imaging

As an imaging adjunct to surgery, MRI is almost ideal: the inherent high contrast of MR images generally offers excellent lesion conspicuity; tomographic images in arbitrary planes, or volume coverage, are available and the potential exists for near continuous imaging for extended periods without concern for dose of ionizing radiation. All of these factors favor MR guidance in interventional applications. On the other hand, interactive control of such procedures demands excellent temporal resolution and visual feedback and only the ultra-fast imaging methods can make truly interventional applications of MRI practical.

One approach to MRI guidance of surgery has been the visualization of laser induced surgical lesions. This work, performed by Ferenc Jolesz, Alan Bleier and their collaborators (96) takes advantage of the high sensitivity and positional specificity of conventional MRI in the visualization of intraparenchymal lesions. At locations planned from the MR images, a surgical Nd:YAG laser is inserted and used to ablate the lesions. Recently this group has utilized Instascan in the *interactive* guidance of the laserthermia surgery (97). Because of the strong dependence the diffusion constant of water on temperature, diffusion-sensitive imaging was used to control the laser dose in real-time, increasing the usable precision of the method in clinical ablations of lesions (figure 26), especially in the central nervous system where considerable hazards exist both from incomplete lesion destruction, and from damage to otherwise healthy tissues. Similar methodology has also been explored by Le Bihan and others (98) for ultrasonically-induced hyperthermia.

4. ALTERNATIVE HIGH SPEED IMAGING METHODS

4.1 Gradient Echoes

While Instascan, and other echo-planar imaging derivatives, are capable of acquiring complete images following a single excitatory pulse, numerous other methods have been proposed and used for scan time reduction. While a comprehensive survey of these would require a review of considerably greater size and scope, we will discuss several recent developments that have pushed imaging times into the ultra-fast domain, and we will contrast these methods with both Instascan and conventional MRI.

The most important alternative techniques, by virtue of their popularity, are the small flip angle gradient echo methods, of which FLASH imaging is the progenitor. Advances in image reconstruction technology have enabled the implementation of a continuous imaging "MR fluoroscopy" mode. In circumstances where operation is constrained to conventional imaging hardware, it may still become practical to utilize echo-planar-like strategies, as in the spiral scan technique described below. The RARE technique is also reviewed briefly, in view of its semi-conventional contrast behavior, its interesting fusion of echo-planar and multiple excitation techniques and its practical application on conventional hardware.

4.1.1 *FLASH and other small flip angle techniques*. Since TR is a primary determinant of overall imaging time, reducing it is an effective scheme for shortening MR acquisition times; FLASH, and its related family of gradient echo imaging methods offer a strategy for TR reduction.

Recall that the MR signal is reduced by repeated excitation; simply decreasing TR in spin echo mode has several consequences: while a two-fold reduction in TR, for example, results in a 50% reduction in scan time, it also results in a reduction of the MR signal due to the reduced longitudinal magnetization of the tissue. Because this magnetization and signal loss is T_1-dependent, reduction of TR adds T_1 contrast to the images. An important development in the reduction of scan times, without this (undesirable) loss of signal, has been the "FLASH" method (99, 100, 101) and the related family of small flip angle techniques, including "FISP"(102), "GRASS"(5), "CE-FAST" (103) etc.

The principle underlying FLASH is straightforward: the MR signal increases with the *sine* of the nutation flip angle (and is largest with a flip angle of 90°) whereas the loss of longitudinal magnetization – or saturation – is proportional to the *cosine* of the flip angle (Figure 27A and 27B). When flip angles of less than 90° are used, and the refocusing pulse is omitted, less magnetization is lost and the signal recovers more rapidly between excitations. As a consequence, it is possible to use shorter TR's with less signal loss than would be seen with 90° flip angles. The key result with FLASH then, is that it is possible to obtain adequate MR signal while minimally disturbing the longitudinal magnetiza-

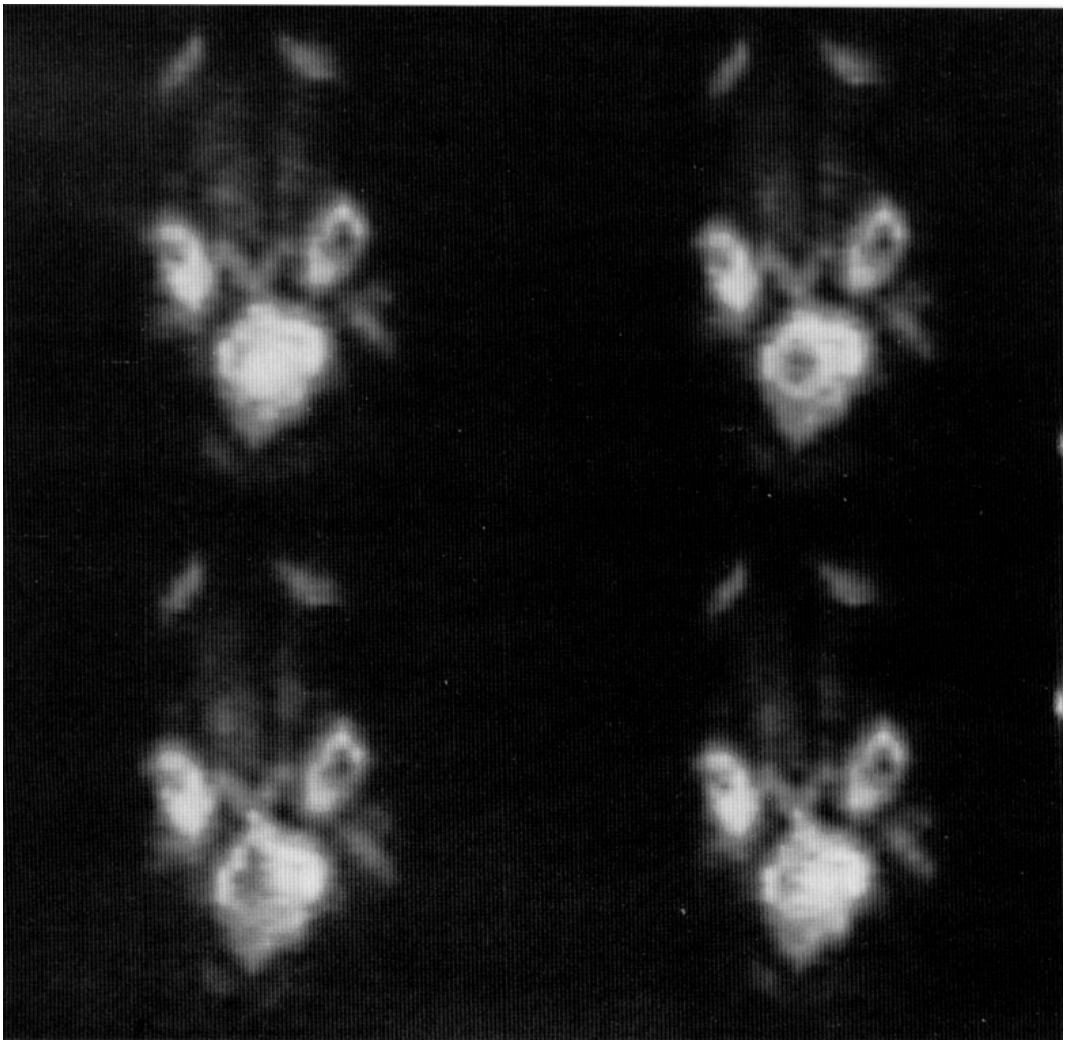

Fig. 26. Diffusion-weighted Instascan images of laser surgery. The high sensitivity of the signal intensity on diffusion-weighted scans to temperature changes has been exploited in the interactive control of experimental laser surgery.[97] Diffusion-weighted scans were acquired once every two seconds before, during and after the laser treatment. The image in the upper left was acquired prior to any laser heating. After six secods of heating with 9 watts of power from a fiber-optically inserted Nd:YAG laser a signal void appears in the image as a consequence of the local increase in diffusion, secondary to the temperature change (upper right). After 20 sec of laser heating the area of reduced signal has grown as shown in the lower left. The brain returns to near normal signal intensity after the laser application has been terminated for 48 sec (lower right). TR: 2 sec; TE: 120 msec; slice thickness: 6 mm; spatial resolution: 1.5 x 3 mm, 128 x 128 matrix. The diffusion-weighted imaging sequence is described in Fig. 23.

tion. As the loss of magnetization is small, the required recovery period is reduced, and shorter repetition times may be utilized. This concept may be extended effectively to the domain of extremely short TR's and small flip angles; recently Haase (104), Atkinson (73, 105), Frahm (106) and others have demonstrated FLASH imaging with TR's of about 4 msec. With flip angles of 5° or less it is possible with this technology to obtain 64 × 128 images in as little as 250 msec (104). Presumably higher resolution scans could be acquired at the cost of longer scan times.

In FLASH imaging the use of 180° refocusing pulses, to form spin echoes, is effectively precluded. The inversion of the longitudinal magnetization these would cause would result in a lengthening, rather than a reduction, in the time required for the recovery of the MR signal. Because there can therefore be no echo-forming pulse, most of these techniques produce "free induction decay" (FID) images: only the gradients are used to rephase the MR signal. For this reason, these are conventionally called "gradient echo" methods. The interval after which the signal is re-formed is called the TE, or echo time. As we will see below, the lack of a refocusing pulse impacts strongly upon the image contrast.

4.1.2 *Contrast behavior of FLASH imaging.* Because the 180° RF pulse is removed, the minimum TE for gradient echo scans is shorter than

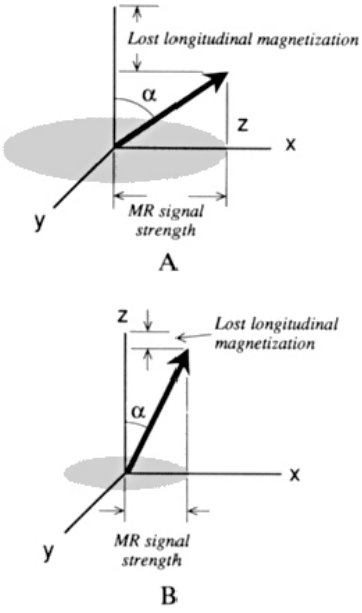

Fig. 27. Principle underlying FLASH and other small flip-angle techniques. (A) A magnetized spin system (shown as a heavy arrow) is represented as a vector in the rotating frame. Following convention, the static field is applied along the *z*-axis. The excitatory RF pulse is applied along the *x* (rotating)-axis and deflects the magnetization, from its equilibrium orientation along the *z*-axis, by a flip angle α into the *x-y* plane. The MR signal, measured as the projection of the vector onto the *x-y* plane, is shown in grey. When α is fairly large, as in this drawing, a large signal is produced at the cost of a significant loss of longitudinal magnetization. The longitudinal magnetization is recovered at the rate T1 as the system returns to the equilibrium condition. Because substantial magnetization is lost with large flip angles this return to equilibrium can require a long recovery period (TR). (B) When somewhat smaller flip angles are used, reasonable signal levels can be produced with substantially less loss of longitudinal magnetization, and the recovery to equilibrium magnetization levels is more rapid. In shallow flip-angle imaging, this is used to advantage by reducing the repetition time, and consequently the overall imaging time.

for their spin echo counterparts. This is advantageous in T_1-weighted scanning, where it is desirable to use short TR's, near the tissue T_1, to maximize T_1 contrast. To minimize T_2 effects (that tend to diminish T_1 contrast) the short TE's are valuable. This short TE advantage of gradient echo scans is to a certain extent mitigated, however, by the relatively rapid T_2* decay (see *"T_2 vs. T_2* Contrast"* below) that adds T_2-like contamination to the images. As an approach to T_1-weighted imaging, the basic FLASH method therefore offers some advantage in reducing the minimum TE and TR. Interestingly, the 180° pulse used in spin echo mode actually reduces the effective TR (for contrast purposes) in conventional spin echo scanning, so that the final decision whether to use FLASH or spin echo imaging for T_1-weighted scans must be based upon a complex tradeoff in imaging time, volume coverage and contrast behavior.

The FLASH imaging strategy wins out particularly when "spin-density" contrast is desired. The spin-density image has minimal contrast contributions from either T_1 or T_2, and has signal intensity determined primarily by the density of protons in each voxel. Because they allow the use of short TR's and TE's without T_1 or T_2 contrast contamination, the FLASH family of methods can reduce the imaging time substantially for these studies.

The newer high speed FLASH studies (104, 106), variously called, "snapshot FLASH" or "Turbo FLASH" or simply "sub-second FLASH", tend to have little contrast, due to their extremely short TR and small flip angle. It is possible, however, to add T_1 contrast by preceding the entire 250 msec acquisition with a 180° inversion pulse (Atkinson 73, 105). As long as the inversion time (TI) is long compared to the data acquisition period this should result in reasonable T_1 contrast. The appearance will be much different, however, than that seen in conventional short TR images. Compared to the single-shot imaging techniques FLASH images show reduced, and somewhat unfamiliar contrast and, in practice it is difficult to achieve T_2-weighting. Nevertheless, sub-second FLASH images are obtained relatively easily on standard imaging hardware and, especially at high field, may demonstrate excellent overall image quality (see Fig. 28).

4.1.3 *Limitations of gradient echo scanning*

4.1.3.1 *Signal-to-noise Ratio Comparisons*. In addition to the contrast differences described above, the theoretically achievable signal-to-noise ratio in Instascan is quite different from that of FLASH or conventional MRI. Since the two methods are presently receiving considerable attention as ultra-fast imaging strategies it is instructive to compare, in an ideal case, the SNR of single-shot imaging and snapshot FLASH for equal resolution cardiac images.

In a well-designed MR instrument, there are three main factors that determine the SNR: voxel size, acquisition time, and transverse magnetization. Larger voxels, longer acquisition periods (i.e. narrower bandwidth) and greater transverse magnetization (90 degree flip angles, short TE to avoid T_2 effects, long TR to avoid saturation, etc…) all tend to increase SNR. For the same voxel size (slice thickness, FOV and resolution) compared to snapshot FLASH, instant scan images tend to be produced with

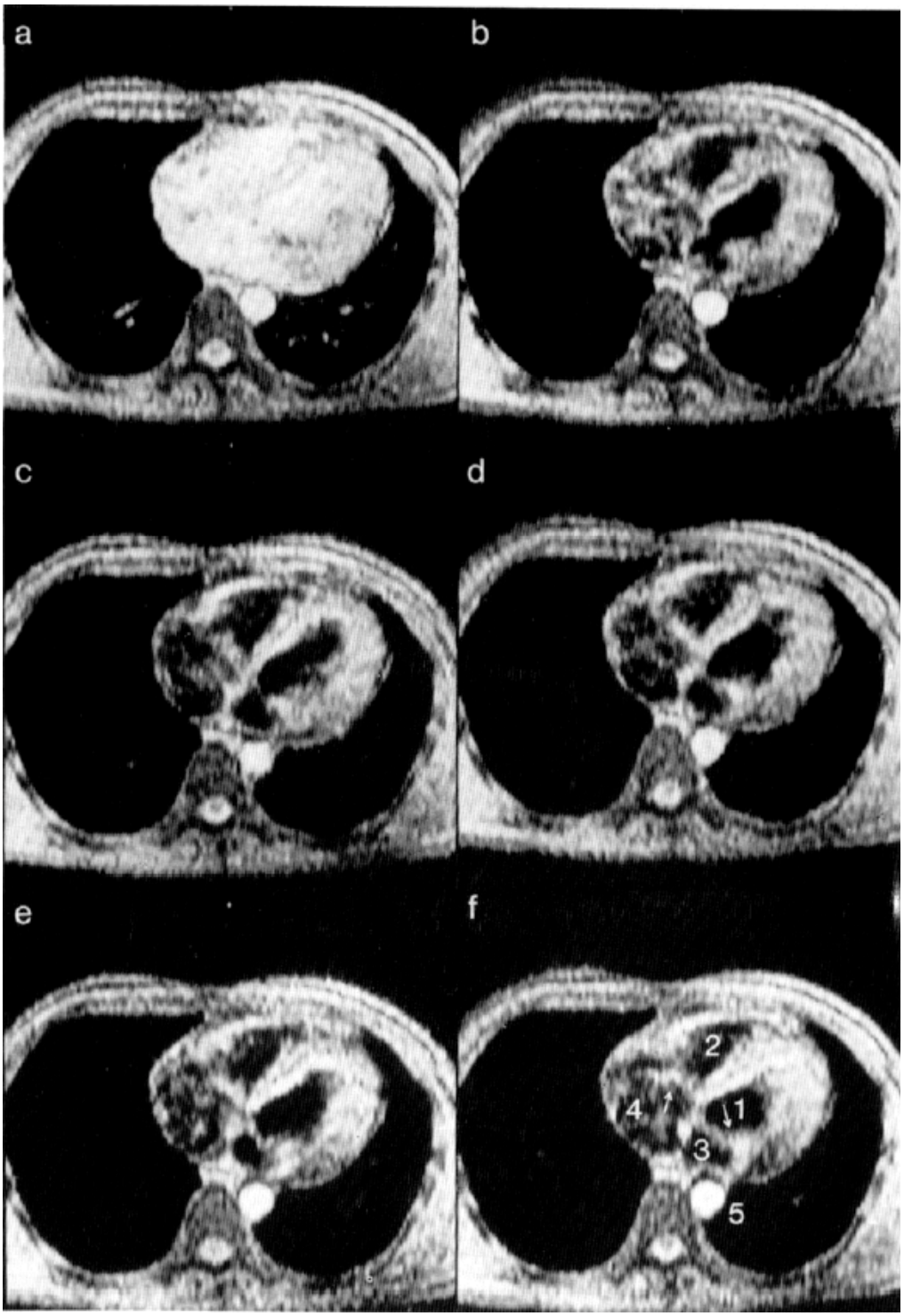

Fig. 28. Subsecond FLASH images. Eighty-five-megahertz (2.0-T) transverse 0.3-s FLASH MR images of the heart of a normal volunteer obtained using the FLASH sequence. The images represent single excitation (unaveraged) scans and have been recorded using the standard circular polarized body coil. The spatial resolution corresponds to 64 x 128 measured dadta points (interpolated to 256 x 256 pixel for display) covering a field-of-view of 250 mm with a slice thickness of 8 mm. The images were selected out of a series of images acquired from different heartbeats without ECG triggering. Without flow suppression (a), flow suppressed images (b)-(f) at different times during the cardiac cycle representing opening (b) and closing (e,f) of the mitral valve. Numbers: 1, left ventricle; 2, right ventricle; 3, left atrium; 4, right atrium; 5, descending aorta. Arrows denote the mitral and tricuspid valves. Reprinted by permission from Frahm, et al., *Magn. Reson. Med.* 13(1): 150-157, 1990.

more net magnetization but are sampled for a shorter period of time. As we will see below, for any reasonable sub-second FLASH image, the

instant scan image will have significantly larger SNR.

Because of the very short TR required, sub-second FLASH images are produced with a shallow (≈ 5 degree) flip angle. The maximum steady-state magnetization available is achieved by exciting at the so-called Ernst angle (after Ernst and Anderson (107)). When TR is very much shorter than T_1, and neglecting the signal losses from T_2*, the resulting transverse magnetization is:

$$SI \sim M_0\sqrt{\frac{TR}{2\,T_1}} \qquad (2)$$

where M_0 is the magnetization that would be available from a fully relaxed spin echo acquisition (see Appendix 1). For example, at 1.5 Tesla, assuming a T_1 for normal myocardium of about 800 msec and a TR of 5 msec (to produce the 300 msec images of Frahm (106)), the transverse magnetization imaged is about 6% of the initial magnetization so that approximately that percentage of the signal is recovered for imaging.

While the Instascan method pays no T_1 penalty (due to its "infinite" TR), the images must be produced at echo times long enough that some transverse (T_2) relaxation losses have occurred. Continuing with the cardiac example above, using either a 40 msec echo with full k-space coverage (cf. section 2.5.3 *"Resolution Improvements"*), or a 20 msec TE with "partial-k" imaging, the effective magnetization diminishes by about 50% with the T_2's present in the myocardium. The Instascan method thus produces a total MR signal about nine times larger than the FLASH technique.

However, we can also show that the FLASH method contributes less noise to the image. While the interactions between gradient amplitude, filter bandwidth and noise amplitude can be subtle, with a few assumptions, the noise can be compared fairly well. If we assume the same field of view and number of pixels in the read direction for the two methods, the effective bandwidth may be contrasted by comparing the acquisition periods. Continuing the sub-second FLASH example above, the acquisition period per line is about 2 msec. In the present Instascan implementation the acquisition period per line is 0.5 msec; but from a noise standpoint, due to the non-linear sampling requirements, the sinusoidal waveform produces an effective period of $(2/\pi) \times 500$ msec ≈ 300 msec. That is, compared to a trapezoidal pulse, the appropriate filter bandwidth must be made wider.

The resulting noise is proportional to the square root of the bandwidth (for the white noise spectrum typical of MR images) and thus inversely proportional to the square root of the sampling period. Using the numbers above, the noise produced is therefore about 2.5 times smaller in the snapshot FLASH images. Combining these three factors (small flip angles for FLASH, longer echo times and wider bandwidth for instant scan), in the heart the overall SNR is from three to four times better with Instascan.

4.1.3.2 *T_2 vs. T_2* Contrast.* Field inhomogeneity within any image voxel results in overall signal loss at the rate T_2* which is, by definition, the combined rate of signal decay from the fundamental T_2 of the sample and the effects of field inhomogeneity (neglecting, for the moment, the effects of diffusion). In general, because of the additional contributions from field inhomogeneity, T_2* is much shorter than T_2; as TE is increased the contrast in gradient echo methods is therefore dominated by T_2* rather than by intrinsic tissue properties. Since an echo-forming RF pulse is not used in small flip angle methods, the resulting scans are sensitive to local variations in magnetic field due to such effects as tissue magnetic susceptibility and to a certain extent magnetic field shimming. For many pathologies, such as multiple sclerosis, most carcinomas, cystic lesions, inflammatory diseases of the skeletal systems, and others, the T_2-weighted scans show better intrinsic contrast than T_1-weighted images. The reduced ability of the gradient echo methods to demonstrate certain pathologies obviates, in many cases, the scan time advantages of the method. In some circumstances, however (*e.g.* Unger *et al.* 108, 109, 110, 111, 112, 113) the enhanced sensitivity of gradient echo scans to susceptibility effects has been used to advantage in clinical diagnostic protocols.

4.1.3.3 *Slice Profiles.* Particularly as the TR is reduced to a few milliseconds, as in the sub-second FLASH scans, the duration of the slice-selective excitation pulse must be reduced, resulting inevitably in compromised slice profiles. As a practical consideration it is therefore difficult to use thin, or closely spaced slices with these methods. A more subtle effect occurs as a result of the dependence of the signal intensity on the combined effects of flip angle and T_1: in tissues with long T_1 outside of the selected plane, the signal may actually be greater than from tissues within the slice. While this problem exists in any small flip angle gradient echo strat-

egy, it becomes increasingly severe as the RF pulse length is reduced.

4.2 Other High Speed Methods

4.2.1 *MR Fluoroscopy*. In the method that Riederer, Farzaneh and coworkers (114, 115) have called "MR Fluoroscopy", the MR data is collected continuously and reconstructed simultaneously. Although the imaging time of 700 msec for 48 × 128 images is just within the ultra-fast domain, the continuous reconstruction yields images relatively free of artifacts in the presence of small or slow motions and may prove a useful tool for its intended applications in continuous imaging and "scout" scans.

4.2.2 *RARE*. RARE (Rapid Acquisition with Refocused Echoes) is another, independent, technique for reducing scan time that is related closely to EPI. In the RARE method, (116. See also Cho *et al.* (117)), multiple RF echoes are formed, each of which is encoded as a separate line of raw data. Each successive line is collected at a later TE and is therefore more T_2-weighted. If the T_2 of the sample is long enough, then many such echoes can be formed. With **n** echoes, an **n**-fold reduction in scan time is achievable. The RARE technique has the disadvantages of somewhat skewed image contrast (since the data are collected at a wide variety of distinct TE's) and relatively high power deposition (owing to the large number of 180° pulses required). It can be used, though, to rapidly produce highly T_2-weighted scans.

4.2.3 *Spiral Scan*. For many applications the most severe motion artifacts are caused by cardiac and respiratory motion. In these applications a single-shot technique may not be necessary; a technique that can produce a set of cardiac-gated images within a breath-holding interval may be sufficient. Meyer, Macovski and Nishimura (42, 47, 118) have studied a technique called interleaved square-spiral fast imaging that produces an image in eight excitations. During each of eight acquisitions the gradients trace out a *k*-space trajectory that constitutes a different square-spiral interleaf as shown in figure 29. Thus they can form a cardiac-gated multi-slice image set or a cardiac movie in a single breath-holding interval.

One advantage of interleaved fast scanning is that the instrumental requirements are eased considerably relative to single-shot techniques. Acquiring the same amount of data during N acquisitions requires $1/N^2$ the gradient power and

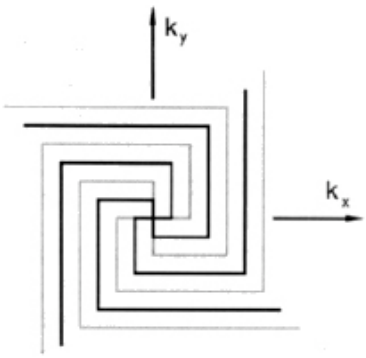

Fig. 29. *K*-space representation of interleaved square-spiral scan (courtesy of Craig Meyer). The interleaved square spiral technique efficiently collects multiple lines of *k*-space following each excitation pulse. To collect sufficient data to form a complete image, eight excitation and data collection cycles are used. The *k*-space spirals following each excitation are interleaved as shown. Because of the square trajectory, relatively little special image processing is required to convert the raw data into images.

1/N the sampling rate and signal bandwidth of a single-shot acquisition. Meyer *et al.* have implemented their eight-shot technique on a commercial GE Signa system with standard gradient amplifiers. Figure 30 shows a single frame from a 17 frame cardiac movie acquired in eight heartbeats. These images were acquired using a water-selective spatial-spectral excitation pulse (50) with a readout time of 34 msec for each acquisition. Other advantages of interleaved fast scanning are √N greater SNR and reduced con-

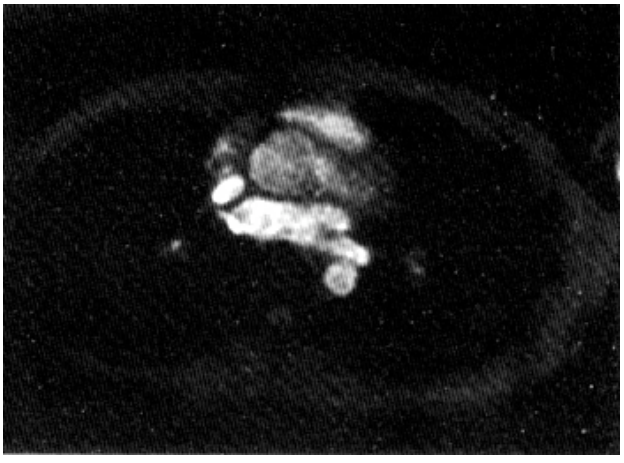

Fig. 30. Cardiac image obtained by interleaved square-spiral scan (courtesy of Craig Meyer). The interleaved square spiral technique has been used to produce good quality cardiac images on a conventional scanner. Because of the relatively long encoding period, which produces a signal bias towards the center of *k*-space, there is a tendency for the small spatial features of tissues with short T2's to be blurred slightly. According to Meyer, one advantage of the square spiral trajectory is its relative resistance to signal dephasing form flow. In these cardiac-gated studies, TR was determined by the subject's heart rate; slice thickness: 10 mm.

cern over potential biological effects from rapidly-switched gradients. Of course, this technique is more susceptible to cardiac arrhythmia and peristaltic motion than single-shot methods.

Spiral *k*-space trajectories as used by Ahn *et al.* (119) and Meyer (118) are an alternative to echo-planar trajectories, chosen primarily for their desirable properties in the presence of flow and T_2 decay. The gradient moments of a spiral trajectory are well-behaved, so that flowing material stays refocused reasonably well during the scan, as shown in the heart image of figure 30. T_2 decay during a spiral scan leads to a loss of resolution that is the same in all directions, that may be preferable to a loss of resolution that is greater in one direction than another, as can occur with other *k*-space trajectories. The main disadvantage of spiral imaging relative to conventional scanning is that the off-resonance species appear blurred in the reconstructed image, instead of being simply shifted along the readout direction (120). The main advantage of the square spiral of figure 29 relative to a round spiral is that the reconstruction can be performed rapidly and accurately by one-dimensional interpolation followed by a 2D fast Fourier transform.

5. THE FUTURE OF ULTRA-FAST MRI

In the thirteen years since Mansfield's original proposal (18) for echo planar imaging, the field of conventional MRI has expanded to become perhaps the most influential modality in radiological diagnostics. By comparison to the conventional methods of multi-shot acquisition, the development of single-shot MRI has lagged, due largely to its technical complexity. Only in the recent years has it become possible to build instruments that achieve medically useful image quality. We expect the applications for such instruments to mushroom in the coming years with growth in three key areas: reduction in scan time for imaging protocols already in clinical use (and resultant decreases in cost); expansion of MRI applications to interactive (e.g. interventional imaging), dynamic and functional assays, and perhaps into non-medical imaging applications such as flow measurement and process and quality control.

Simple scan time reduction is important as the physician can generally defend the purchase of capital equipment only on the basis of validated clinical utility: it is therefore crucial that the instruments produce images with contrast and sensitivity closely analogous to that of accepted protocols. For the moment, the physician is generally most comfortable with spin echo contrast, though the gradient echo methods are becoming increasingly accepted. For similar reasons, and for the validation of high-speed protocols, it is important that the equipment be capable of collecting conventional images.

As an example of the key clinical applications for the ultra-fast methods, we expect to see a growth in rapid whole body examination where preliminary data (Cohen, Rosen, *et al.* unpublished observations) show that the entire body can be covered in thin slice T_2-weighted spin echo images in under fifteen minutes (of which less than the five minutes is actual imaging – the rest being related strictly to mechanical issues such as repositioning the patient.) The ready availability of high performance computing machinery allows the physician to rapidly reformat these data into preferred viewing planes. Such data sets would have applications in screening procedures, potentially replacing methods such as whole body scintigraphy as a cancer screen while providing the radiologist with the additional anatomic resolution and sensitivity of conventional MRI.

Many publications have indicated that orthopedic and cardiac diagnosis (e.g. 5, 121) is facilitated by collecting a time series of images that display tissue in motion. The real-time methods available with ultra-fast MRI should greatly expand the use of MRI for dynamic functional assessment both in orthopedic applications and in evaluation of soft tissue organ systems (e.g. swallowing and gastrointestinal studies).

As complete examination times are reduced to a few minutes, we expect that the physician's involvement with the scanning process must change as well. Already, highly interactive user interfaces are being explored (122, Stehling, *personal communication,* 123) with which the physician may adjust scan planes, oblique orientation, and other key imaging parameters such as TR, TI and TE with trackballs or soft knobs. Inevitably, this functionality will imply either greater involvement by the radiologist in the scanning process, or a greatly increased responsibility for the radiological technologist: with the capability to collect hundreds of images per minute the exams must be well targeted simply to avoid the collection of overwhelming quantities of data.

This enormously increased rate of MR data collection will have tremendous implications in the methods of storing, recalling and presenting MR images. Presently, the digital media (magnetic disks and tapes, or optical disks) are either too slow or too expensive for the practical handling of ultra-fast imaging data. In the short-term, therefore, we can anticipate a shift to

video tape data storage that, in turn, puts an increasing burden on the supporting computer equipment to provide real-time image processing of the raw MR data. There must also be significant improvements in data compression and automated analysis and reduction simply to keep up with the inflow of medical data.

As tremendous gains have been made in the applications, quality and acceptance of conventional MRI, ultra-fast imaging has quietly evolved from theoretical possibility, to working prototype, to emerging clinical reality. As the first few instruments are introduced into clinical institutions, we may see yet another revolution in the practice of radiology.

APPENDIX

DERIVATION OF THE SIGNAL PRODUCED IN FLASH IMAGING.

According to Weber (124), the signal intensity (SI) produced in FLASH imaging is:

$$SI = M_0 \sin\alpha \left(\frac{1 - e^{-TR/T_1}}{1 - \cos\alpha\, e^{-TR/T_1}}\right), \qquad (A1)$$

where M_0 is the initial longitudinal magnetization and α is the RF flip angle. At the Ernst angle, where the FLASH signal is maximized,

$$\cos\alpha = e^{-TR/T_1}. \qquad (A2)$$

Substituting equation A2 into A1 we find that

$$SI = M_0 \left(\frac{1 - \cos\alpha}{\sin\alpha}\right) \qquad (A3)$$

$$= M_0 \tan\left(\frac{\alpha}{2}\right). \qquad (A4)$$

When α is small, and when TR << T_1, we can make the approximations:

$$\cos\alpha \sim 1 - \frac{\alpha^2}{2} \qquad (A5)$$

and

$$e^{-TR/T1} \sim 1 - \frac{TR}{T_1}. \qquad (A6)$$

The Ernst condition implies that equation A5 is equal to equation A6. Combining these two equations and solving for $\alpha/2$ we find that:

$$\frac{\alpha}{2} \sim \sqrt{\frac{TR}{2T_1}}. \qquad (A7)$$

For small angles we can approximate $\tan\alpha = \alpha$. Thus, substituting equation A7 into A4:

$$SI \sim M_0 \sqrt{\frac{TR}{2T_1}}. \qquad (A8)$$

REFERENCES

1. Evens RG, Jost RG and Evens RG. Economic and utilization analysis of magnetic resonance imaging units in the United States in 1985. American Journal of Radiology 145:393-398 (1985).
2. Ehman RL, McNamara MT, Brasch RC, Felmlee JP, Gray JE and Higgins CB. Influence of physiologic motion on the appearance of MR images. Radiology 159:777-782 (1986).
3. Henkelman RM, Bronskill MJ. Artifacts in magnetic resonance imaging. Reviews of Magnetic Resonance in Medicine. 2(1):1-126 (1987).
4. Wood ML, Runge VM and Henkelman RM. Overcoming motion in abdominal MR imaging. American Journal of Roentgenology 150:513-522 (1988).
5. Glover GH and Pelc NJ. A rapid gated cine MRI technique. In: Kressel HY ed. Magnetic resonance annual 1988. New York:Raven 299-333 (1988).
6. Turner R and Le Bihan D Single-shot diffusion imaging at 2.0 Tesla. Journal of Magnetic Resonance. 86:445-452 (1990).
7. McKinstry RC, Weisskoff RM, Cohen MS, Vevea JM, Kwong KK, Rzedzian RR, Brady TJ, Rosen BR. Instant MR Diffusion/Perfusion Imaging. Magnetic Resonance Imaging 8(Suppl) No. 401 (1990).
8. Bloch F. Nuclear induction. Physical Review 70:460-474 (1946).
9. Hahn EL. Spin echoes. Physical Review 80:580-594 (1950).
10. Bottomley PA, Foster TH, Argersinger RE and Pfeiffer LM. A review of normal tissue hydrogen NMR relaxation times and relaxation mechanisms from 1-100 MHz: dependence on tissue type, NMR frequency, temperature, species, excision and age. Medical Physics 11:425 (1984).
11. Bottomley PA, Hardy CJ, Argersinger RE, Allen-Moore G. A review of 1H nuclear magnetic resonance relaxation in pathology: are T1 and T2 diagnostic?. Medical Physics 14(1):1-37 (1987).
12. Brown TR, Kincaid BM and Ugurbil K. NMR chemical shift imaging in three dimensions. Proceedings of the National Academy of Science. 79:3523 (1982).
13. Twieg DB. Acquisition and accuracy in rapid NMR imaging methods. Magnetic Resonance in Medicine. 2:437-452 (1985).
14. Twieg DB. The k-trajectory formulation of the NMR imaging process with applications in analysis and synthesis of imaging methods. Medical Physics. 10:610-621 (1983).

15. Ljunggren S. A simple graphical representation of Fourier-based imaging methods. Journal of Magnetic resonance. 54:338-343 (1983).
16. Bracewell RN. The Fourier Transform and its Applications. 2d Edition. New York:McGraw Hill (1978).
17. Margosian PM. Faster MR imaging - imaging with half the data. Society for Magnetic Resonance in Medicine (abstr) No. 1024 (1985).
18. Mansfield P. Multi-planar image formation using NMR spin echoes. Journal of Physics C10, L55-L58, (1977).
19. Mansfield P and Pykett IL. Biological and medical imaging by NMR. Journal of Magnetic Resonance 29:355-373 (1978).
20. Chapman B, Turner R, Ordidge RJ, Doyle M, Cawley M, Coxon R, Glover P and Mansfield P. Real-time movie imaging from a single cardiac cycle by NMR. Magnetic Resonance in Medicine 5:246-254 (1987).
21. Ordidge RJ, Coxon R, Howseman A, Chapman B, Turner R, Stehling M and Mansfield P. Snapshot head imaging at 0.5 T, using the echo planar technique. Magnetic Resonance in Medicine 8:110-115 (1988).
22. Stehling MJ, Howseman AM, Ordidge RJ, Chapman B, Turner R, Coxon R, Glover P, Mansfield P and Coupland RE. Whole-body echo-planar MR imaging at 0.5 T. Radiology 170:257-263 (1989b).
23. Rzedzian RR and Pykett IL. An instant technique for real-time MR imaging (abstr). Radiology 161(P): 333, (1986).
24. Pykett IL and Rzedzian RR. Applications and performance of the instant technique in the body. Society for Magnetic Resonance in Medicine, works in progress (abstr.) No. 10 (1987).
25. Pykett IL and Rzedzian RR. Instant images of the body by magnetic resonance. Magnetic Resonance in Medicine 5:563-571 (1987).
26. Rzedzian RR and Pykett IL. Instant images of the human heart using a new, whole-body MR imaging system. American Journal of Roentgenology 149:245-250 (1987).
27. Rzedzian RR. A method for instant whole-body MR imaging at 2.0 Tesla and system design considerations in its implementation. Society for Magnetic Resonance in Medicine Abstracts. #229 (1987).
28. Tropper MM. Image reconstruction for the NMR echo-planar technique and for a proposed adaptation to allow data acquisition. Journal of Magnetic Resonance 42:193-202 (1981).
29. Bruder H, Fischer H, Schmitt F and Reinfelder H -E. Reconstruction procedures for Echo Planar Imaging. Society for Magnetic Resonance in Medicine (abstr) No. 359 (1989).
30. Schmitt F, Fischer H and Görtler G. Useful filterings and phase corrections for EPI derived from a calibration scan. Society for Magnetic Resonance Imaging, works in progress (abstr.) no. 464 (1990).
31. Rzedzian RR. Real time MRI at 2.0 Tesla. Society for Magnetic Resonance in Medicine Abstracts. #247 (1988).
32. Cohen MS, Weisskoff RM and Rzedzian RR. Clinical Methods for "Single-Shot" Instant MR Imaging of the heart. Radiology (abstr) 173(P):359 (1989a).
33. Wedeen VJ, Crawley AP, Weisskoff RM, Holmvang G and Cohen MS. Real time MR imaging of structured fluid flow. Submitted to Society of Magnetic Resonance in Medicine (1990).
34. Bydder GM and Young IR. MR imaging: clinical use of the inversion recovery sequence. Journal of Computer Assisted Tomography 9(4):659-675 (1985).
35. Weisskoff RM, Cohen MS and Rzedzian RR. Fat suppression techniques: a comparison of results in instant imaging. Society for Magnetic Resonance in Medicine Abstracts. #836 (1989).
36. Stehling MK, Ordidge RJ, Coxon R and Mansfield P. Inversion-recovery echo planar imaging (IR-EPI) at 0.5 T. Magnetic Resonance in Medicine. 13(3):514-517 (1990).
37. Lauterbur PC. NMR zeugmatographic imaging by true three-dimensional reconstruction. Journal of Computer Tomography 5:285 (1981).
38. Cohen MS and Rohan ML. 3D volume imaging with Instant Scan. Society for Magnetic Resonance in Medicine (abstr) No. 831 August (1989).
39. Cohen MS, Dalcanton JJ, Weisskoff RM, Rohan ML. Kinematic imaging of the knee using instant MRI. *Presented at*: Society of Magnetic Resonance in Medicine. (1990b).
40. Rohan ML. Practical limits to gradient coil design. Society for Magnetic Resonance in Medicine Abstracts. #963 (1989).
41. Dickinson RJ, Goldie F, and Firmin D. Gradient power requirements for echo-planar imaging. Society for Magnetic Resonance in Medicine (abstr) No. 828 August (1989).
42. Macovski A and Meyer CH. Gradient power and T2 considerations in rapid imaging. Society for Magnetic Resonance in Medicine (abstr) No. 449 (1987).
43. Rzedzian RR. Method of high speed imaging with improved spatial resolution using partial k-space acquisitions. US patent no. 4,767,991 (1988).
44. Rzedzian RR. High speed, high resolution, spin echo imaging by Mosaic scan and MESH. Society for Magnetic Resonance in Medicine Abstracts. #51 (1987).
45. Weisskoff RM, Dalcanton JJ and Cohen MS. High Resolution 64 msec Instant Images of the Head. Magnetic Resonance Imaging 8 (suppl. 1):93 (1990a).
46. Farzaneh F, Riederer SJ, Maier JK and Vavrek R. View-interleaved EPI on a commercial scanner. Society of Magnetic Resonance in Medicine (abstr.) 832 (1989).
47. Macovski A and Meyer CH. A novel fast scanning system. Society for Magnetic Resonance in Medicine (abstr) No. 156 (works in progress) (1986).

48. Hore PJ. Solvent suppression in Fourier transform nuclear magnetic resonance. Journal of Magnetic Resonance. 55:283-300 (1983).
49. Weisskoff RM. Improved hard-pulse sequences or frequency-selective presaturation in magnetic resonance. Journal of Magnetic Resonance. 86:170-175 (1990).
50. Meyer CH, Pauly JM, Macovski A and Nishimura DG. Simultaneous spatial and spectral selective excitation. Magnetic Resonance in Medicine 15(2):287-304 (1990).
51. Reilly JP. Peripheral nerve stimulation by induced electric currents: exposure to time-varying magnetic fields. Medical & Biological Engineering and Computing **27**, 101-110 (1989).
52. Reilly JP. Peripheral nerve stimulation and cardiac excitation by time-varying magnetic fields: a comparison of thresholds. Report MT90 - 100 for The Office of Science and Technology, Center for Devices and Radiological Health, US Food and Drug Administration. April, (1990).
53. Bourland JD, Mouchawar GA, Nyehuis JA, Geddes LA, Foster KS, Jones JT, Graber GP. Transchest magnetic (eddy-current) stimulation of the dog heart. Medical and Biological Engineering and Computing 28:196-198. (1990)
54. Cohen MS, Weisskoff RM, Rzedzian RR, Kantor HL. Sensory stimulation by time-varying magnetic fields. Magnetic Resonance in Medicine 14:409-414 (1990a).
55. Cohen MS, Weisskoff RM, Kantor HL. Evidence of peripheral stimulation by time-varying magnetic fields. Radiology (abstr) 173(P):382 (1989b).
56. Fischer H. Physiological effects by fast oscillating magnetic field gradients. Radiology (Abstr) 173(P) #382 (1989).
57. Farzaneh F, Riederer SJ and Pelc NJ. Analysis of T2 limitations and off-resonance effects on spatial resolution and artifacts in echo-planar imaging. Magnetic Resonance in Medicine 14:123-149 (1990).
58. Weisskoff RM and Rzedzian RR. High-resolution instant images in the brain. Radiology 173(P):1272 (1989).
59. Levin DN. Neurosurgical applications of integrated 3D display of MRI and PET. Society for Magnetic Resonance Imaging (abstr) No. PS20 (1990).
60. Villringer A, Rosen BR, Belliveau JW, Ackerman JL, Lauffer RB, Buxton RB, Chao Y-S, Wedeen VJ and Brady TJ. Dynamic imaging with lanthanide chelates in normal brain: contrast due to magnetic susceptibility effects. Magnetic Resonance in Medicine 6:164-174 (1988).
61. Rosen BR, Belliveau JW, Betteridge D, Cohen MS, Weisskoff RM, Vevea JM, RR. Perfusion imaging with magnetic-susceptibility contrast media. Radiology (abstr) 173(P):383 (1989).
62. Rosen BR, Belliveau JW, Vevea JM and Brady TJ. Perfusion imaging with NMR contrast agents. Magnetic Resonance in Medicine 14(2):249-266 (1990).
63. Rosen BR, Belliveau JW and Chien D. Perfusion Imaging by Magnetic Resonance. Magnetic Resonance Quarterly. Vol 5, No. 4:226-281 (1990).
64. Kantor HL, Rzedzian RR, Pykett IL, Berliner E, Brady TJ, Buxton R. Transient effects of gadolinium-DTPA and dysprosium-DTPA intravenous infusion on myocardial NMR image intensity using high speed NMR imaging. Society of Magnetic Resonance in Medicine (abstr.) No. 246 (1988).
65. Kantor HL, Rzedzian RR, Berliner E, Beaulieu P, Buxton RB, Brady TJ and Pykett IL. A new NMR marker of coronary stenoses: the utility of dysprosium-DTPA in high speed cardiac imaging. Society of Magnetic Resonance in Medicine (abstr.) No. 803 (1988).
66. Kantor HL, Rzedzian RR, Berliner E, Beaulieu P, Brady TJ and Pykett IL. Detection of coronary stenoses by high speed NMR imaging: the utility of dysprosium-DTPA. In: Proceedings of the American College of Cardiology Annual Meeting (1989)
67. Belliveau JW, Villringer A, BR, Lauffer RB, Ackerman JL, Buxton R, Frazer J, Johnson K, Moore J, Wedeen VJ and Brady TJ. Magnetic susceptibility induced signal attenuation changes in rat brain caused by hypercapnia. Society of Magnetic Resonance Imaging in Medicine, works in progress (abstr.) p 273 (1986).
68. Belliveau JW, Kantor HL, Pykett IL, Rzedzian RR, Berliner E, Beaulieu P, Buonanno FS, Brady TJ and Rosen BR. Real-time proton susceptibility-contrast imaging of cerebral physiology. Society of Magnetic Resonance Imaging in Medicine (abstr.) No. 222 (1988).
69. Belliveau JW, Kantor HL, Pykett IL, Rzedzian RR, Beaulieu P, Kennedy DN, Fisel CR, Brady TJ and Rosen BR. Real-time proton susceptibility-contrast imaging of hypercapnia induced changes in cerebral physiology. Society of Magnetic Resonance Imaging in Medicine (abstr.) No. 222 (1988).
70. Belliveau JW, Rosen BR, Buxton RB, Johnson KA, Frazer JC, Moore JB, Chao Y-S, Garrido L, Lauffer RB, Fisel CR and Brady TJ. Dynamic imaging with gadolinium of magnetic susceptiblility contrast effects in experimental brain ischemia. Society of Magnetic Resonance Imaging in Medicine, works in progress (abstr.) p. 7 (1987).
71. Belliveau JW, Rosen BR, Kantor HL, Rzedzian RR, Kennedy DN, McKinstry RC, Vevea JM, Cohen MS, Pykett IL and Brady TJ. Functional cerebral imaging by susceptibility-contrast NMR. Magnetic Resonance in Medicine 14(3):538-546 (1990).
72. Stehling MK, Bullock P, Firth JL, Blamira AM, Ordidge RJ, Coxon R, Gibbs P and Mansfield P. Gd-DTPA real-time studies of the brain with EPI: a dynamic approach to perfusion and blood-brain barrier assessment. Society for Magnetic Resonance in Medicine (abstr) No. 358. August, (1989a).

73. Atkinson DJ, Burstein D and Edelman RR. First-pass cardiac perfusion: evaluation with ultrafast MR imaging. Radiology 174:757-762 (1990).
74. Le Bihan D, Breton E, Lallemand D, Grenier P, Cabanis E, Laval-Jeantet M. MR imaging of intravoxel incoherent motions: application to diffusion and perfusion in neurologic disorders. Radiology 161:401-407 (1986).
75. Stejskal EO, Tanner JE. Spin diffusion measurements: spin echoes in the presence of a time-dependent field gradient. Journal of Chemical Physics 42:288-292 (1965).
76. Drucker E, Pykett IL, Rzedzian RR, Miller S and Dinsmore RE. Preliminary evaluation of a new high-speed MR imaging system for the assessment of cardiac function in normal volunteers. Society for Magnetic Resonance in Medicine (abstr) No. 17 August (1987).
77. Wood ML and Henkelman RM. Magnetic resonance artifacts from periodic motion. Medical Physics 12:143-151 (1985).
78. Stark DD, Wittenberg J, Edelman RR, Middleton MS, Saini S, Butch RJ, Brady TJ, Ferrucci JT. Detection of hepatic metastases: analysis of pulse sequence performance in MR imaging. Radiology 159:365-370 (1986).
79. Haacke EM, Lenz GW. Improving MR image quality in the presence of motion by using rephasing gradients. American Journal of Radiology 148:1251-1258 (1987).
80. Runge VM, Clanton JA, Partain CL, James AE. Respiratory gating in magnetic resonance imaging at 0.5 Tesla. Radiology 151:521-523 (1984).
81. Ehman RL, McNamara MT, Pallack M, Hricak H, Higgins CB. Magnetic resonance imaging with respiratory gating: techniques and advantages. American Journal of Roentgenology 143:1175-82 (1984).
82. Vinitski S, Mitchell DG, Burk DL, Rifkin MD, Levy D, Szumoski U. Fat and motion artifact suppression in combined gradient and spin echo (GREASE) technique. Society of Magnetic Resonance in Medicine abstr. 1025 (1988).
83. Felmlee JP and Ehman RL. Spatial presaturation: a method for suppressing flow artifacts and improving detection of vascular anatomy. Radiology 164:559-564 (1987).
84. Bailes DR, Gilderdale DJ, Bydder GM, Collins AG, Firmin DN. Technical Note. Respiratory ordered phase encoding (ROPE): a method for reducing phase encoding artefacts in MR imaging. Journal of Computer Assisted Tomography 9:835-838 (1985).
85. Nishimura DG, Macovski A and Pauly JM. Magnetic resonance angiography. IEEE transactions on medical imaging. vol. MI-5(3):140-151 (1986).
86. Pattany PM, Phillips JJ, Lee CC, Lipcamon JD, Durek JL, McNally JM and Mohapatra SN. Motion artifact suppression technique (MAST) for MR imaging. Journal of Computer Assisted Tomography 11(3):369-377 (1987).
87. Stehling MK, Evans DF, Lamont , Ordidge RJ, Howseman AM, Chapman B, Coxon R, Mansfield P, Hardcastle JD and Coupland RE. Gastrointestinal tract: dynamic MR studies with echo-planar imaging. Radiology 171:41-46 (1989c).
88. Saini S, Stark DD. Rzedzian RR, Pykett IL, Rummeny E, Hahn PF, Wittenberg J and Ferrucci JT. Forty-millisecond imaging of the abdomen at 2.0 T. Radiology 173:111-116 (1989).
89. Stark DD, Pykett IL, Rzedzian RR, Wittenberg J, Ferrucci JT. Millisecond imaging at 2.0 tesla. Society for Magnetic Resonance in Medicine, works in progress (abstr.) No. 11 (1987).
90. Dumoulin CL and Hart HR. Magnetic Resonance Angiography. Radiology 161:717-720 (1986).
91. Wedeen VJ, Meuli RA, Edelman RR, Frank LR, Brady TJ, Rosen BR. Projective imaging of pulsatile flow with magnetic resonance. Science 230:946-948 (1985).
92. Laub GA and Kaiser WA. MR angiography with gradient motion refocusing. Journal of Computer Assisted Tomography 12(3):377-382 (1988).
93. Cohen MS and Crawley AP. Time-resolved MR angiography using real-time MRI. submitted for publication. (1990).
94. Cohen MS. High-speed MR imaging: from fast to instant. Magnetic Resonance Imaging 8 (suppl. 1):177 (1990).
95. Keller PJ, Drayer BP, Fram EK, Williams KD, Dumoulin CL and Souza SP. MR angiography with two-dimensional acquisition and three-dimensional display. Works in Progress. Radiology 173(2):527-532 (1989).
96. Jolesz FA, Bleier AR, Jakab P, Ruenzel PW, Huttl K, Jako GJ. MR imaging of laser-tissue interactions. Radiology 168(2):249-253 (1988).
97. Bleier AR, Panych L, Cohen M, Weisskoff R, Dalcanton J, Hushek S, Higuchi N, Rosen B, McKinstry RM and Jolesz FA. Visualization of Laser Heat Propagation with Instant Imaging. Society for Magnetic Resonance Imaging (abstr) No. 416, February, (1990).
98. Le Bihan D, Delannoy J, Levin RL. Temperature mapping with MR imaging of molecular diffusion: application to hyperthermia. Radiology 171:853-857 (1989).
99. Frahm J, Haase A, Matthaei. Rapid three-dimensional imaging using the FLASH technique. Journal of Computer Assisted Tomography 10(2):363-368 (1986).
100. Frahm J, Haase A, Matthaei KD. Rapid NMR imaging of dynamic processes using the FLASH technique. Magnetic Resonance in Medicine 4:162-174 (1987).

101. Haase A, Frahm J, Matthaei KD. FLASH imaging: rapid NMR imaging using low flip angles. Journal of Magnetic Resonance 67:258-266 (1986).
102. Oppelt A, Graumann R, Barfuss H, Fischer H, Hartl W and Schajor W. FISP - a new fast MRI sequence. Electromedica 54:15-18 (1986).
103. Gyngell ML. Steady-state free precession sequences. Topical Conference on Fast Magnetic Resonance Imaging Techniques (abstr.) (1987).
104. Haase A. Snapshot FLASH MRI. Applications to T1, T2 and chemical-shift imaging. Magnetic Resonance in Medicine 13:77-89 (1990).
105. Atkinson DJ and Edelman RR. Ultrafast 2D cardiac imaging. Society of Magnetic Resonance Imaging in Medicine (abstr.) 137 (1988).
106. Frahm J, Merboldt KD, Bruhn H, Gyngell ML, Hänicke W and Chien D. 0.3-second FLASH MRI of the human heart. Magnetic Resonance in Medicine 13(1):150-157 (1990).
107. Ernst RR and Anderson WA. Application of Fourier transform spectroscopy to magnetic resonance. Reviews of Scientific Instruments 37:93-102 (1966).
108. Unger EC, Cohen MS and Brown TR. Gradient echo imaging of hemorrhage at 1.5 Tesla. Magnetic Resonance Imaging 7(3):163-172 (1989a).
109. Unger E, Darkazanli A and Cohen M. Fast MR scanning reduces artifacts in the abdomen. Diagnostic Imaging 11(11):248-256 (1989b).
110. Unger EC, Cohen MS, Gatenby RA, Clair MR, Brown TR, Nelson SJ and McGlone JS. Single Breath-holding scans of the abdomen using FISP and FLASH at 1.5 Tesla, Journal of Computed Tomography 12(4):575-583 (1988).
111. Unger EC, Cohen MS and Brown TR. FISP and FLASH of hemorrhage. Magnetic Resonance Imaging vol. 5 suppl. 1 (1987).
112. Atlas SW, Mark AS, Fram EK. Aqueductal stenosis: evaluation with gradient-echo MR imaging. *Radiology* 169:449-453 (1988a).
113. Atlas SW, Mark AS, Fram EK, Grossman RI. Vascular intracranial lesions: applications of gradient-echo MR imaging. *Radiology* 169:455-461 (1988b).
114. Riederer SJ, Tasciyan T, Farzaneh F, Lee JN, Wright RC and Herfkens RJ. MR fluoroscopy: technical feasibility. Magnetic Resonance in Medicine 8:1-15 (1988).
115. Farzaneh F, Riederer SJ, Lee JN, Tasciyan T, Wright RC, Spritzer CE. MR fluoroscopy: initial clinical studies. Radiology 167:541 (1988).
116. Hennig J, Nauerth A, and Friedburg H. RARE imaging: a fast method for clinical MR. Magnetic Resonance in Medicine. 3:823-833 (1986).
117. Cho ZH, Hilal SK, Kim HS and Song HB. Computer modeling and simulation of Fourier transformation NMR imaging. In: Partain et al. ed. Nuclear magnetic resonance imaging. Philadelphia:Saunders 453-486 (1983).
118. Meyer CH, Macovski A, Nishimura DG. Square spiral fast imaging. Society for Magnetic Resonance in Medicine (abstr) No. 362 (1989).
119. Ahn CB, Kim JH and Cho ZH. IEEE Transactions on Medical Imaging MI-5(1):2-5 (1986).
120. Meyer CH and Macovski A. Square spiral fast imaging: interleaving and off-resonance effects. Society for Magnetic Resonance in Medicine (abstr) No. 230 (1987).
121. Niitsu M, Akisada M, Anno I and Miyakawa S. Moving knee joint: technique for kinematic MR imaging. Radiology 174:569-570 (1990).
122. Holsinger AE, Wright RC, Riederer SJ, Farzaneh F, Grimm RC and Maier JK. Real-time interactive magnetic resonance imaging. Magnetic Resonance in Medicine 14:547-553 (1990).
123. Weisskoff RM, Dalcanton JJ and Rzedzian RR. 40 millisecond instant long axis heart imaging. To be presented at: Society of Magnetic Resonance in Medicine (1990b).
124. Weber H, Purdy D, Deimling M, Oppelt A. Contrast behaviour ofthe fast imaging sequences FLASH and FISP: results from synthetic images. Society of Magnetic Resonance in Medicine abstr. 957-958 (1986).